buildings

MDPI

Article

Experimental and Numerical Investigation of the Shear Performance of PSCC Shear Connectors with Poured UHPC

Fengli Zhou [1], Chunwu Guo [2], Jiangtao Zhang [1], Jincen Guo [1,3,*], Jinlong Jiang [1] and Lulin Ning [4]

[1] State Key Laboratory of Mountain Bridge and Tunnel Engineering, Chongqing Jiaotong University, Chongqing 400074, China
[2] Hainan Province Road-Bridge Construction Investment Group Co. 2, Hainan 570100, China
[3] Department of Civil Engineering, School of Civil and Transportation Engineering, Shenzhen University, Shenzhen 518060, China
[4] China Shipbuilding Industry Corporation Haizhuang Wind Power Co., Chongqing 401123, China
* Correspondence: gjc@mails.cqjtu.edu.cn; Tel.: +86-18720936427

Abstract: Assembled steel-composite bridges generally use stud connectors to achieve the connection between the deck slab and the steel main girders. However, the commonly-used cluster studs weaken the integrity of the precast deck slabs and are not conducive to reducing the size of the precast deck slabs. Based on the excellent mechanical performance of UHPC, a precast steel-concrete composite bridge system consisting of precast bridge deck slabs, bonding cavities, and steel girders was proposed in this study. The system was named PSCC (Precast Steel-Concrete Connectors). To verify the applicability of PSCC connectors in engineering, push-out tests and finite element analysis were carried out in this paper to investigate the shear performance and influence parameters of PSCC connectors. The results showed that compared with the full bonding at the steel-UHPC interface, the shear bearing capacity of the specimens with 30% debonded area rate (the ratio of defect area to total interface area) and the shear bearing capacity of the specimens with 60% debonded area rate decreased by 0.35% and 9.74%, the elastic stiffness decreased by 14.86% and 21.72%, and the elastic-plastic stiffness decreased by 1.6% and 12.8%, respectively. When the steel-UHPC percentage of debonded area is less than 30%, the shear resistance of PSCC connectors is affected very little. However, when the steel-UHPC percentage of debonded area is 60%, the shear resistance of PSCC connectors is greatly affected. Therefore, adequate filling of the UHPC connection layer should be ensured in the project. In addition, the PSCC connectors have excellent ductility, their characteristic slip value S_u is much higher than the EC4 specification of 6 mm, and they have better shear performance than conventionally installed stud connectors. According to the results of the parametric analysis, it was found that the failure mode of the PSCC connectors was shear reinforcement fracture when the area ratio of shear reinforcement to stud was less than 1.55, under the premise of the same material strength. On the contrary, the failure mode of PSCC connections was stud fracture. When the transverse spacing of both studs and shear reinforcement is 4d, the PSCC connectors can maintain a high ultimate load capacity while reducing the amount of UHPC in the bonding cavity. Therefore, 4d was chosen as the best spacing for both studs and shear reinforcement.

Keywords: finite element model; composite structure; ultra-high-performance concrete; push-out test; stud connector

Citation: Zhou, F.; Guo, C.; Zhang, J.; Guo, J.; Jiang, J.; Ning, L. Experimental and Numerical Investigation of the Shear Performance of PSCC Shear Connectors with Poured UHPC. *Buildings* **2023**, *13*, 212. https://doi.org/10.3390/buildings13010212

Academic Editor: Mohamed K. Ismail

Received: 24 November 2022
Revised: 30 December 2022
Accepted: 4 January 2023
Published: 12 January 2023

1. Introduction

Steel-concrete composite bridges can take full advantage of the respective material properties of steel and concrete. Steel-concrete composite bridges are widely used in bridge engineering because of their light weight, load-bearing capacity, excellent fatigue resistance, and significant comprehensive economic benefits [1,2]. Traditional steel-concrete composite beams use the cast-in-place construction method to splice steel main girders and bridge slabs. However, cast-in-place concrete increases the construction duration and is influenced

by the construction environment, and ultimately, structural quality [3]. Compared with the former, the on-site assembly connection construction method has the advantages of reliable quality, shorter construction duration, and less interference with existing traffic because the main components of the assembled combination bridge are prefabricated rather than cast-in-place [4–6]. Nowadays, assembled bridge construction technology is also more mature, allowing for block-by-block adjustments of prefabricated formwork that can accommodate a variety of complex line shapes and installations. However, the mechanical performance and structural design of shear connectors in assembled structures affect the mechanical properties and construction efficiency of assembled composite bridges [7–9]. Therefore, research on shear connectors has been a major topic in assembled composite structures.

Shear connectors are set on the top plate of the steel beam to transfer the internal forces between the steel beam and the concrete. Shear connectors enable the steel beam and concrete deck slab to work together and to prevent the two members from sliding against each other and the concrete from lifting upwards. The main mechanical performance includes load-bearing capacity, stiffness, and ductility [10–12]. Generally, the connectors need to have a high bearing capacity, mainly to reduce the number of connectors. The connectors also need to be sufficiently stiff and ductile, with the main purpose of avoiding excessive structural slip during the serviceability stage, as well as the ability to redistribute the load at the ultimate limit state or to prevent unexpected shock loads from causing the connection to fail. In addition, the shear connectors in prefabricated assembled composite bridges should meet the mechanical performance requirements while also being adapted to the construction of assembled bridges, mainly in the form of simple connection structures and fast assembly of prefabricated bridge decks to avoid uncontrollable quality caused by cast-in-place concrete. With reliable connection, convenient on-site construction, and excellent structural performance, stud connectors have become the most widely used assembly connectors. However, the limited load bearing capacity of stud connectors and the dense arrangement lead to usually large reserved hole sizes, which weaken the concrete slab significantly [13,14]. The stud connectors within normal concrete require a sufficient thickness of the protective layer of the precast deck slab, thus preventing further light weighting of the precast deck slab. Ultra-High Performance Concrete (UHPC) is a much better-performing concrete material [15,16] with very high compressive strength, excellent tensile strength, and good ductility, durability, and fluidity [17–19], and has been widely used in engineering structures [20,21]. The use of UHPC as cast-in-place material can greatly improve the connection performance of shear connectors and reduce the dimensional limitations of precast bridge decks, thereby reducing dead weight.

The shear performance of stud connectors in UHPC has been extensively studied. Fang et al. [22] conducted 18 push-out tests and analyzed the UHPC casting method, stud diameter, UHPC plate thickness, interface shape, and stud arrangement variation as the primary study parameters. Based on the experimental results, an accurate calculation model was proposed to predict the ultimate shear strength and load-slip curves of the stud connectors in steel-UHPC prefabricated composite slabs. Tong et al. [23] conducted six push-out tests to investigate the shear performance of the stud connectors with different stud diameters and layout forms. The other arrangement of studs had little effect on their shear performance, and after changing the material to high-strength steel and UHPC, the former had almost no effect. The latter significantly improved the shear bearing capacity and shear stiffness of the connector, but the ductility was relatively poor. Kim et al. [24] conducted 15 push-out tests with different parameters to demonstrate the feasibility of UHPC thin plates. The results showed that the length-diameter ratio of the stud could be reduced from 4 to 3.1 without affecting the stud shear strength. UHPC slabs do not develop splitting cracks after the UHPC layer is reduced to 25 mm. Wang et al. [25] investigated the shear performance of studs in UHPC and therefore analyzed a series of parameters, including the diameter of the studs, the length-diameter ratio of the studs, the strength of plain concrete and the strength of UHPC. The results show that UHPC can resist high lateral splitting forces at the root of the stud. UHPC is better matched to large-diameter studs stud

connectors with the length-diameter ratio of 2.3 and can have sufficient strength in UHPC plates. Zou et al. [26] proposed a new type of assembled connector construction of PCSC, which has obvious advantages in construction compared with cast-in-place connectors and conventional assembled connectors. PCSC connector has a sufficient load-bearing capacity reserve and excellent deformation capacity in the deformation of the load. The construction technology reduces the difficulty of prefabrication and assembly of concrete components and reduces the construction duration. The above study shows that the stud connectors in UHPC have excellent mechanical performance.

The application of UHPC in assembled composite bridges can significantly improve the connection performance of the stud connectors. Therefore, based on the connection advantages of the existing stud connectors in UHPC, a newly assembled steel-concrete shear connector (PSCC) is proposed in this paper. To investigate the mechanical performance of PSCC connectors, three groups of static push-out tests were conducted. The mechanical properties of PSCC connectors under monotonic loading were investigated using the parameters of the steel-UHPC interface bonding state, and the failure modes of the specimens were determined. Finally, the PSCC shear connectors model is established and verified with the experimental results compared against each other. The analysis of shear reinforcement diameter, shear reinforcement spacing, and stud spacing parameters was performed on a model matching the test results.

2. PSCC Connector

2.1. Structural Design

Figures 1 and 2 show the PSCC (Prefabricated Steel-Concrete Connection) connector, which mainly consists of three parts: studs, pre-embedded shear steel members, and UHPC bonding material. The detailed construction of this shear connection in the assembled steel-concrete composite bridge is as follows: first, side baffles are welded on both sides of the upper flange of the steel girder to ensure that the UHPC is filled in the bonding cavity between the precast bridge deck and the steel girder. At the same time, studs are welded on the top of the upper flange of the steel girder to ensure the internal force transfer between the UHPC and the steel girder. Secondly, the pre-embedded steel members comprise shear reinforcement and sealing steel plates. With the sealing steel plate as the boundary, the top of the shear reinforcement is pre-embedded in the prefabricated bridge deck slab to realize the internal force transfer between the prefabricated bridge deck slab and the UHPC. Finally, after the precast deck plate is installed on the steel girder, the sealing steel plate, side baffles, and the upper flange of the steel girder form the bonding cavity. After the deck plate and steel girders are installed in place, the UHPC is filled in the reserved holes of the deck plate, and the bonding cavity is fully wrapped with studs and bottom shear reinforcement, thus realizing the shear force transfer form of the precast deck plate—UHPC bonding material—steel girders.

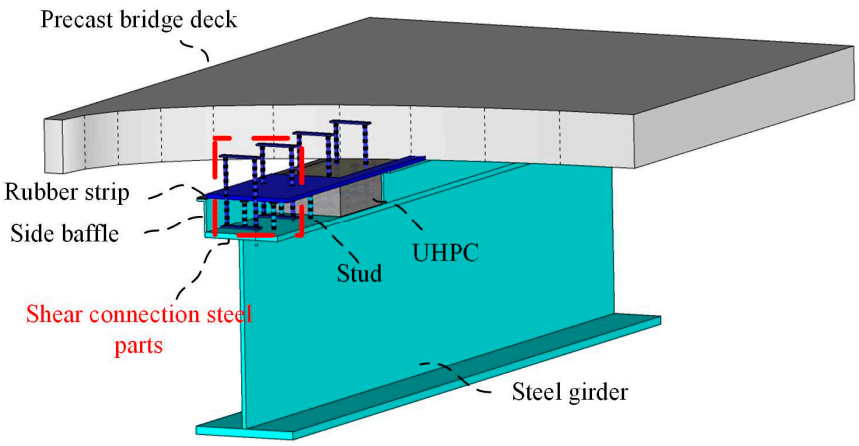

Figure 1. Three-dimensional sketch of PCSC connectors.

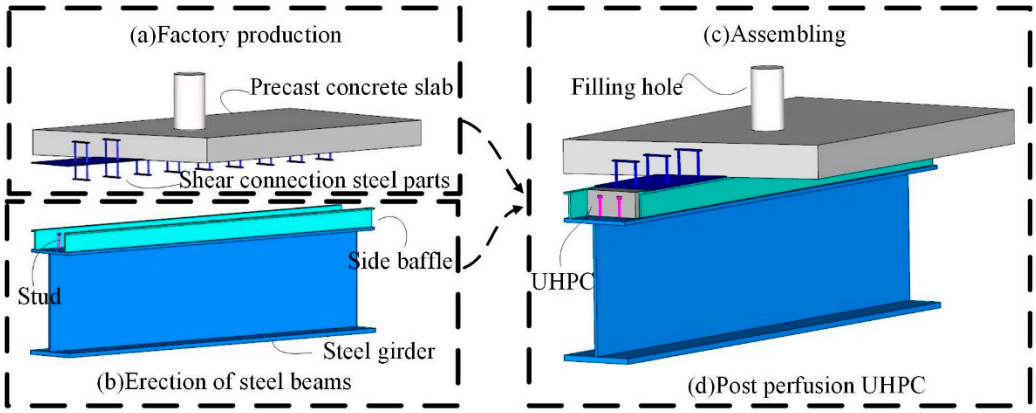

Figure 2. Design of PSCC connectors.

2.2. Structural Features

Depending on the assembly process in a real bridge, the PSCC connector is divided into two parts: the deck plate section with the shear connection steel member and the steel girder section with side baffles and studs. The load is transferred from the prefabricated deck slab to the bonding cavity section and then to the steel girders via shear reinforcement and studs. PSCC connectors offer an efficient assembly process and superior performance, the main advantages of which can be classified as follows:

(1) PSCC shear connectors do not change the structure of prefabricated bridge decks and do not require slotting to cause weak areas in the deck, ensuring the overall performance of the deck.
(2) During the bridge deck slab's installation, the sealing steel plate was in the middle of the shear connection steel member. This permitted to convert the traditional connection between precast concrete and steel girders into a kind of connection between steel structures during alignment. The whole bridge deck slab and the shear connection steel member were made in the factory, thus significantly improving the matching accuracy during installation.
(3) Based on the superb mechanical properties of UHPC, the reliability of the connection between the studs and the pre-embedded steel members can be ensured, and the shear force transfer path is clarified to ensure the designability of this shear connection.

3. Experiment Program

3.1. Design of Specimens

The specimens were designed according to the EC4 specification [27], and the specimens were partially adjusted according to the relevant requirements of the test. The dimensions of the specimens are shown in Figures 3 and 4. The precast concrete members in the push-out test are uniformly rectangular members of 150 mm × 400 mm × 420 mm. To prevent the load eccentricity situation during the test, the steel members are designed as box types, with a box section of 50 mm × 138 mm, top and bottom plate section of 12 mm × 182 mm, and web section of 12 mm × 50 mm. The length of the side baffle is 360 mm, and the section size is 6 mm × 40 mm. The top of the side baffle is equipped with a sealing steel plate for the shear steel member, with a length of 360 mm and a cross-sectional dimension of 4 mm × 218 mm. The sealing steel plate may slip during the loading process, so a 30-mm vacancy is preset in the precast concrete slab. A rubber strip is provided on the top surface of the side baffle to prevent the grouting of UHPC from leaking. The test's shear studs are unified with a stud shank diameter of 13 mm, length of 52 mm, stud cap diameter of 22 mm, and length of 8 mm. The whole arrangement is three rows of two columns, stud center transverse spacing of 65 mm, and longitudinal spacing of 100 mm. The shear reinforcement is 12 mm in diameter, 170 mm in length, 65 mm in transverse

spacing, and 100 mm in longitudinal spacing, staggered with studs and joined together by a sealing steel plate.

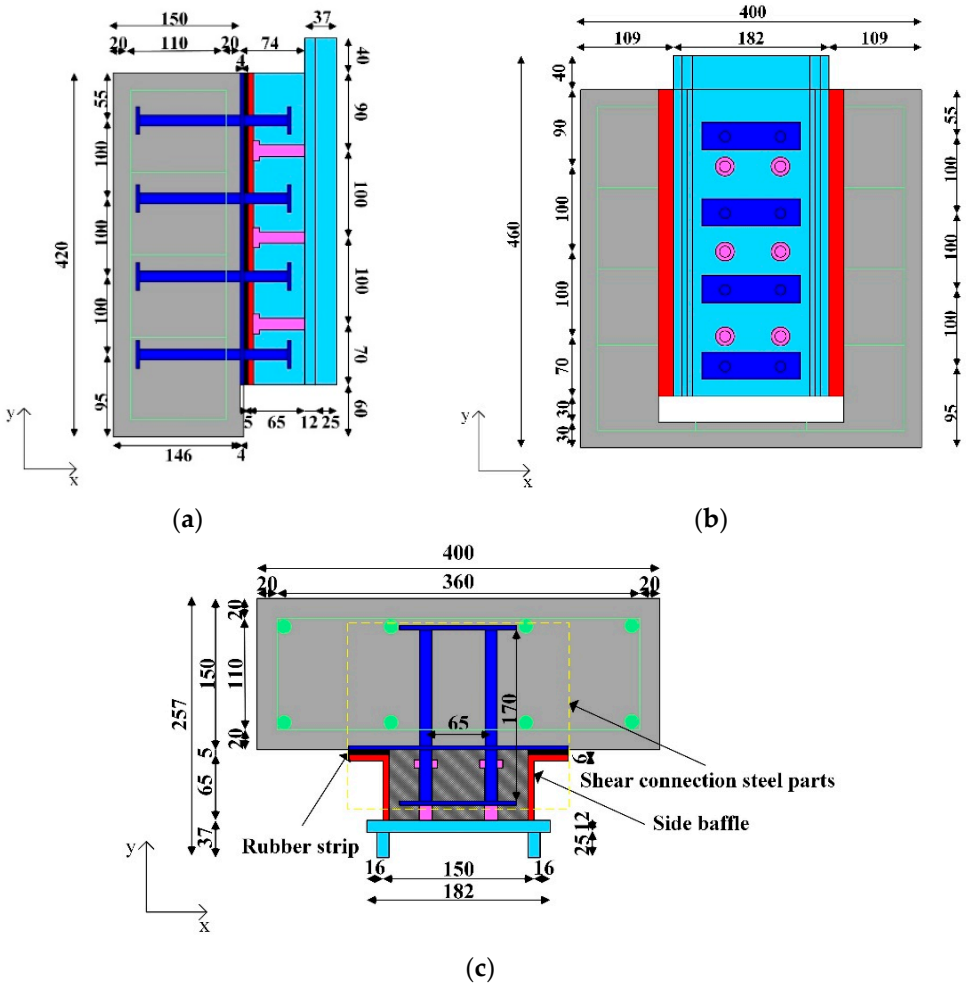

Figure 3. Details of specimens: (**a**) Front view; (**b**) Side view; (**c**) Top view. (Unit: mm).

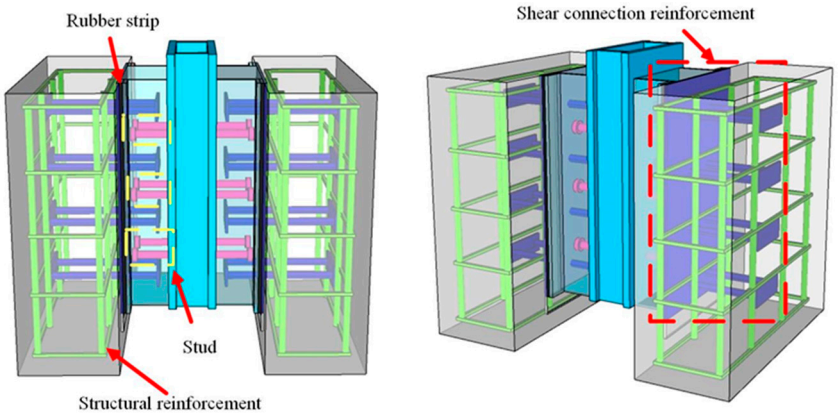

Figure 4. Three-dimensional of the specimen.

When the bridge deck plate and steel girders are spliced and completed in real bridge construction, the UHPC is poured afterward through the pre-drilled holes. The bonding force of the steel-UHPC interface is weakened because of the insufficient denseness of the UHPC in the bonding cavity. Therefore, the specimen design considered the influence of the steel-UHPC interface state on the shear performance of the connector. A total of three groups of six specimens were designed and produced for this test, with two specimens

in each group, and Table 1 shows the grouping of the specimens. The interface defect arrangement is shown in Figure 5.

Table 1. Grouping of push-out test specimens.

Specimen	Percentage of Debonded Area	No. of Tests	Description
ZC	0	2	Impact of interface defects
TK30	30%	2	
TK60	60%	2	

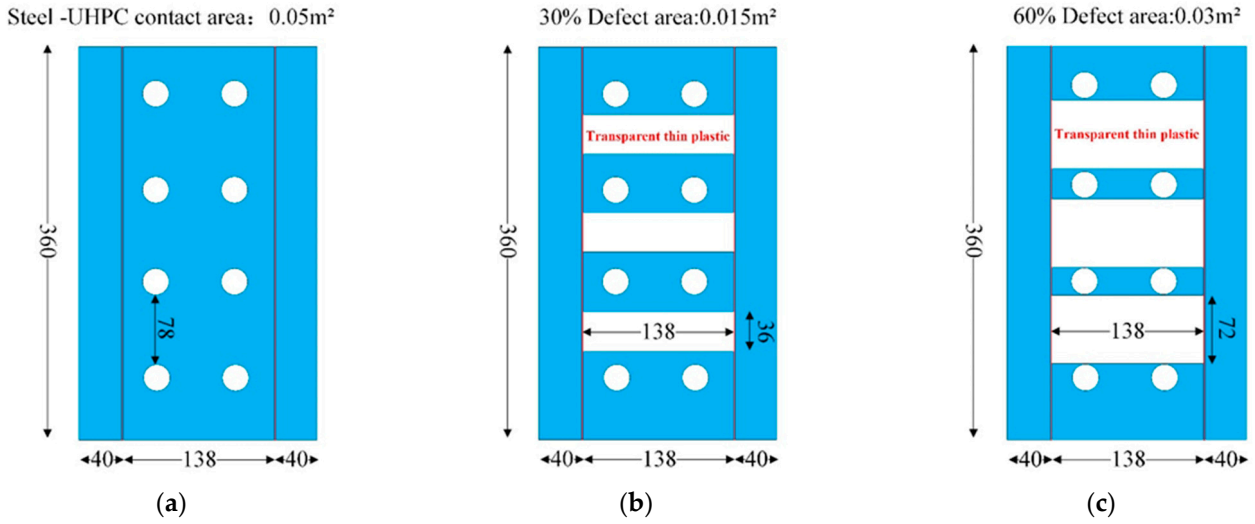

Figure 5. Steel-UHPC interface defect layout: (**a**) full bond; (**b**) 30% interface defects; (**c**) 60% interface defects.

3.2. Fabrication of Specimens

As shown in Figure 6, the whole component can be divided into seven steps: 1. Wooden molds for precast concrete slabs were made and pre-built shear connection steel parts were machined. The sealing steel plates of shear connection steel members of ZC group specimens did not need to be processed while sealing steel plates of shear connection steel members of TK group specimens needed to be processed to simulate steel-UHPC interface defects after the completion of area allocation according to the specified calculation. The thin transparent tape was bonded to the steel plate. Finally, the shear connection steel members were assembled into the prefabricated formwork. 2. Constructional reinforcing steel was tied, and formwork was erected. 3. Precast concrete slabs were poured and maintained. 4. Fabrication of steel members and welding of studs. The steel members were fabricated in the factory, and the welding studs were welded using the ceramic ring protection welding method. 5. To ensure a tight bond between the precast concrete layer and the steel members, rubber strips were pasted on the side baffles, followed by assembling the precast concrete members with the steel members. 6. After the assembly was completed, the whole specimen was fixed with thick wire to prevent leakage during the concrete pouring. 7. The bonding cavity was poured with UHPC.

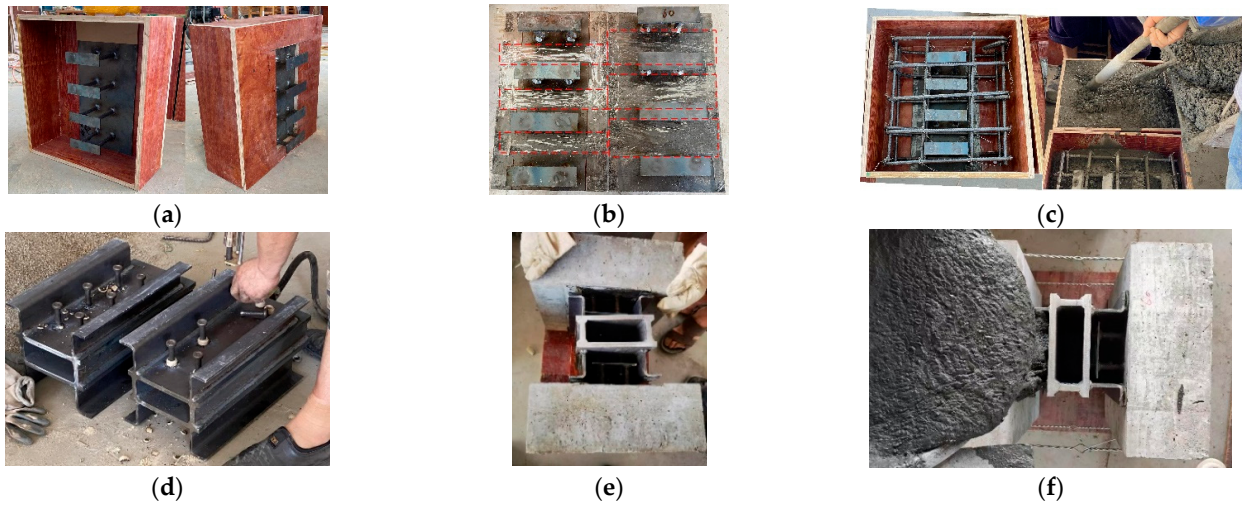

Figure 6. Fabrication procedures of specimen: (**a**) Formwork of precast slab; (**b**) Defect arrangement; (**c**) Casting concrete; (**d**) Welding stud; (**e**) Assemble; (**f**) Pouring connection concrete.

3.3. Materials

The precast concrete used in this test was C50. All steel plates used Q355C grade steel. Shear reinforcement and structural reinforcement used HRB400. All ordinary concrete materials in this study were of C50 grade. All steel was Q355C steel with a nominal yield strength of 355 MPa. All reinforcements were HRB400, and UHPC with good fluidity was used for the bonding cavity. The mechanical properties of the concrete, steel bar, and steel plate involved in the test were selected according to the Chinese standards, "Standard for test methods for mechanical properties on ordinary concrete" (GB/T50081-2016) [28] and "Standard for Metallic materials-Tensile testing-Part 1: Method of test at room temperature" (GB/T228-2010) [29]. Their specific tests were obtained, as shown in Figure 7, and the particular performance parameters are shown in Table 2.

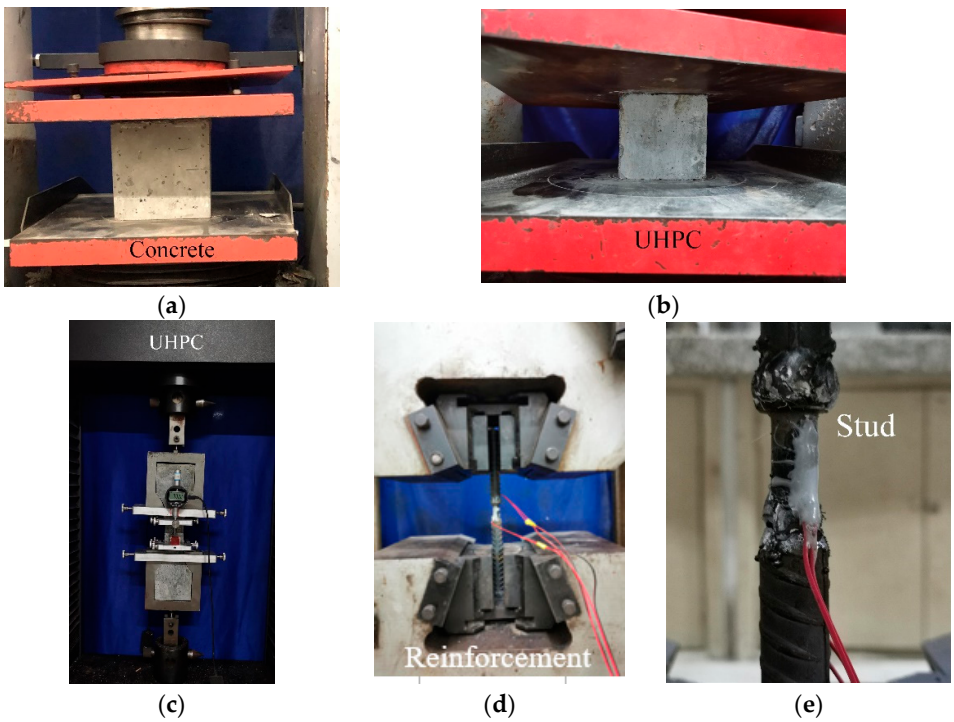

Figure 7. Testing of material properties:(**a**) Concrete; (**b**) UHPC; (**c**) UHPC; (**d**) Reinforcement; (**e**) Stud.

Table 2. Material properties of specimens.

Material	Fcu (Mpa)	Ec (Gpa)	Fy (Mpa)	Fu (Mpa)	Es (Gpa)
C50	45	36	-	-	-
UHPC	120	40	-	-	-
Q355C	-	-	355	450	210
HRB400	-	-	416	564	209
Stud	-	-	430	480	210

Note: "-" means no measurement data, because this material does not require this indicator.

3.4. Loading Method and Instrument Layout

The test specimens were loaded by a 1000 T microcomputer-controlled electro-hydraulic servo press for static monotonic loading. A layer of fine sand was evenly laid at the bottom of the specimen and the loading steel plate. Three preloads, with an amplitude of 0.3 times the predicted ultimate load, were applied before the formal loading to eliminate the gap between the specimen and the press and to check whether the measuring equipment was working correctly [30]. After completing the preloading, the test was controlled by force loading at 2 kN/s, as shown in Figure 8. The pressure transducer reads the applied load on the specimen. Figure 9 shows the four displacement transducers used for measuring the relative slip between the steel box and the precast concrete slab. The relative slip between the UHPC and the precast concrete slab was measured using two displacement transducers.

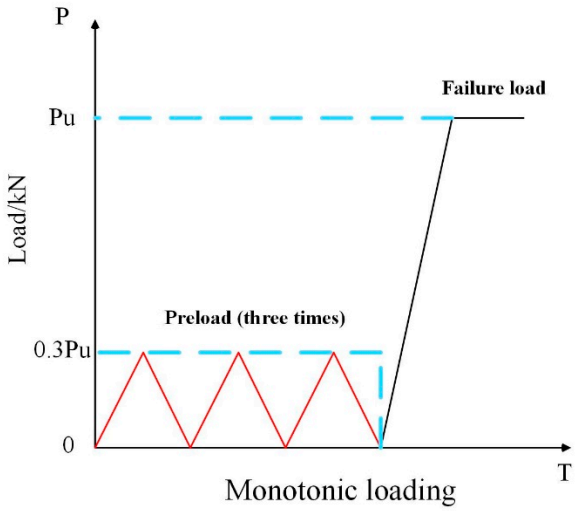

Figure 8. Loading procedure for push-out tests.

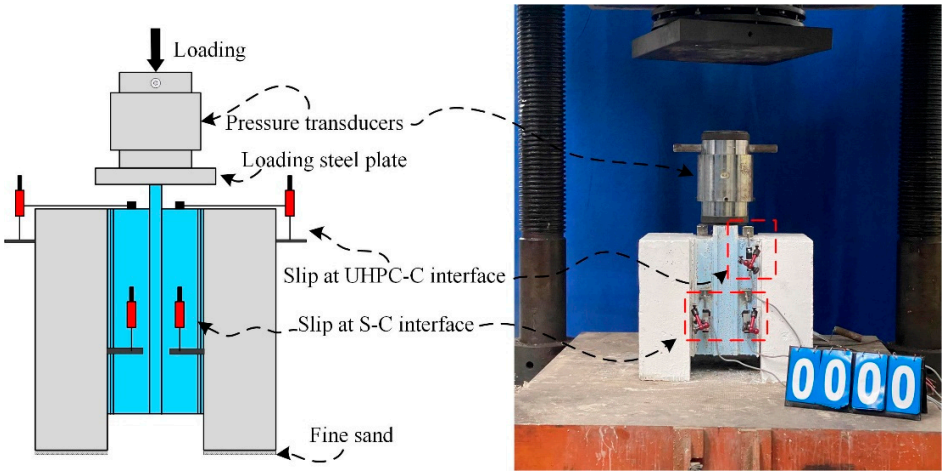

Figure 9. Test setup and layout of displacement transducer.

4. Experiment Results

4.1. Failure Modes

All the push-out specimens showed similar failure modes. The ZC-1 (naturally bonding) specimen was chosen as a representative to describe the experimental process. Slips between steel box and precast concrete slabs and slips between precast concrete slabs and UHPC layers were measured in this study. The test results showed that the shear connection steel member and the precast concrete slab were completely bonded together, and there was no slip between them at the end. The C-UHPC interface did not slip significantly during the whole loading process. At the final failure, the interior of the UHPC layer was cut off, so the slip measured at the top of the UHPC was null. Therefore, the subsequent analysis was performed by the relative slip of the steel box-precast concrete slab interface.

At the initial loading stage, no cracks were generated at the precast slab, and no slip appeared at the interface of the UHPC and precast concrete slab, but the slip at the interface of steel and the precast slab grew slowly. When the load reached 0.47 Pu (Ultimate load capacity), a micro crack appeared on the right side of the precast slab. Later, as the load increased, the cracks gradually extended upward to both sides. When the load reached 0.87 Pu, a small slip appeared at the steel-UHPC interface. Subsequently, when the steel-concrete slab slip reached 3 mm, the whole member continued to sound like concrete cracking. When the slip reached 7.5 mm, and the load reached the Pu, the specimen produced a loud sound. However, the steel-UHPC interface was not immediately damaged, and a steady decrease in bearing capacity occurred after a certain degree of interface slip. Finally, the slip at the interface of the steel box and precast plate kept increasing. The specimen emitted a continuous ringing sound until the loading stopped after the load suddenly dropped to 0.6 Pu. The loading process is shown in Figure 10.

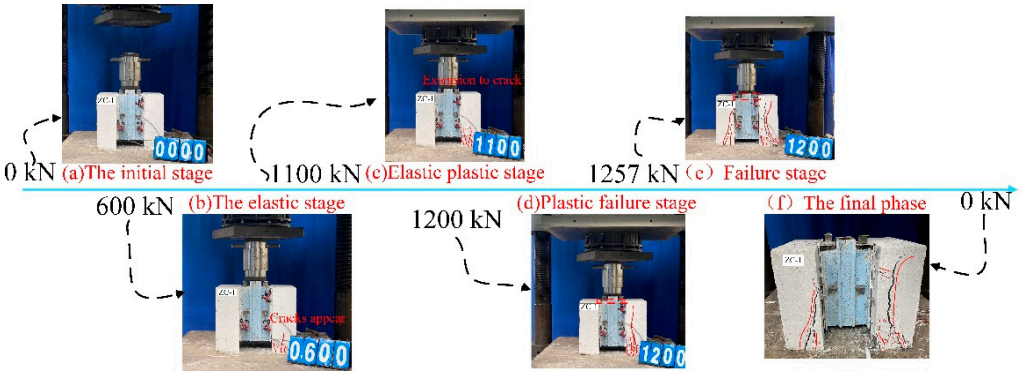

Figure 10. Main test phenomena of ZC-1 specimen.

This test had three groups of specimens, including ZC group specimens, TK30 group specimens, and TK60 group specimens. The specimens in the ZC group were naturally bonded at the steel-UHPC interface, the specimens in the TK30 group were bonded at the steel-UHPC interface with a 30% debonded area rate (ratio of defect area to total interfacial area), and the specimens in the TK60 group were bonded at the steel-UHPC interface with a 60% debonded area rate. The failure mode of the PSCC shear connectors was shear reinforcement fracture as shown in Figure 11. The ZC group specimen showed that the shear reinforcement embedded in the bonding cavity was fractured from the root. The UHPC was compressed due to deformation of the shear reinforcement, thus leaving marks on the sealing steel plate. Despite the high strength of the UHPC, the UHPC layer broke as a whole from the inside in the final failure result. The shear reinforcement in the bonding cavity fractured sequentially from the bottom up. Despite the steel-UHPC interface defects, there was no significant difference between the failure modes of the TK30 group specimens and TK60 group specimens. However, there was a significant decrease in the ultimate bearing capacity for the steel-UHPC interface defects. The failure of each group of the specimen was shown as shown in Figure 12.

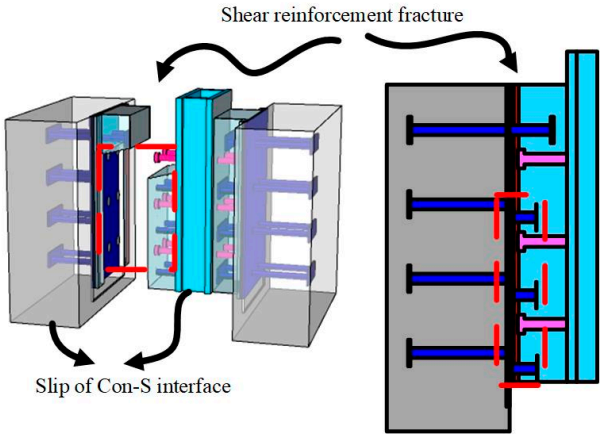

Figure 11. Typical failure form of specimens.

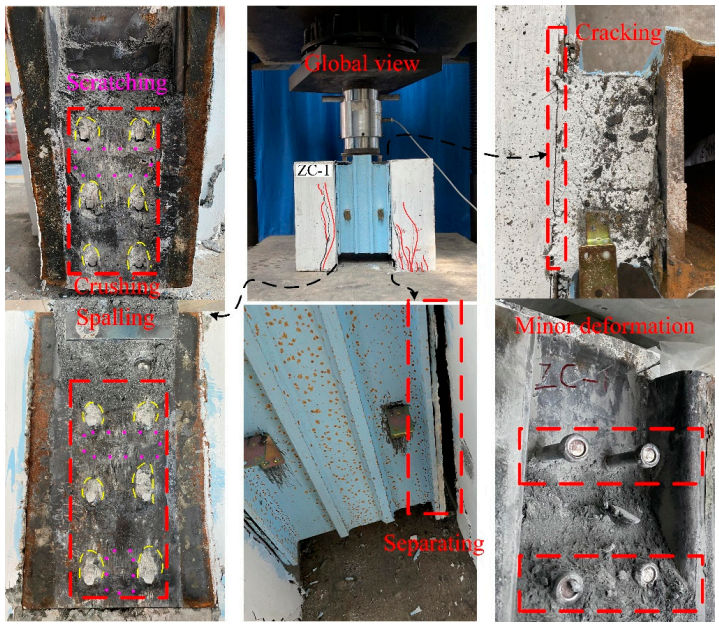

Figure 12. *Cont*.

(**c**)

Figure 12. Failure state of specimens:(**a**) Failure form of specimens of ZC group; (**b**) Failure form of specimens of TK30 group; (**c**) Failure form of specimens of TK60 group.

4.2. Load-Slip Curves

The slip at the steel–precast concrete slab interface was the average of the data measured by four displacement transducers before and after. The applied load of the specimen was measured by the force transducer. Figure 13a–c shows the load-slip curves of each specimen in the three groups. Under monotonic loading, the failure modes of the ZC, TK30, and TK60 groups are mainly shear reinforcement shear fractures. As can be seen from Figure 13, all specimens can be divided into three stages: the elastic stage (0 Pu~0.4 Pu), the elastic-plastic stage (0.4 Pu~0.91 Pu), and the plastic failure stage (0.91 Pu~Pu). For the three groups of specimens, there is a plastic stage at the steel-concrete interface where the bearing capacity does not change significantly, but the interface slip continues to grow.

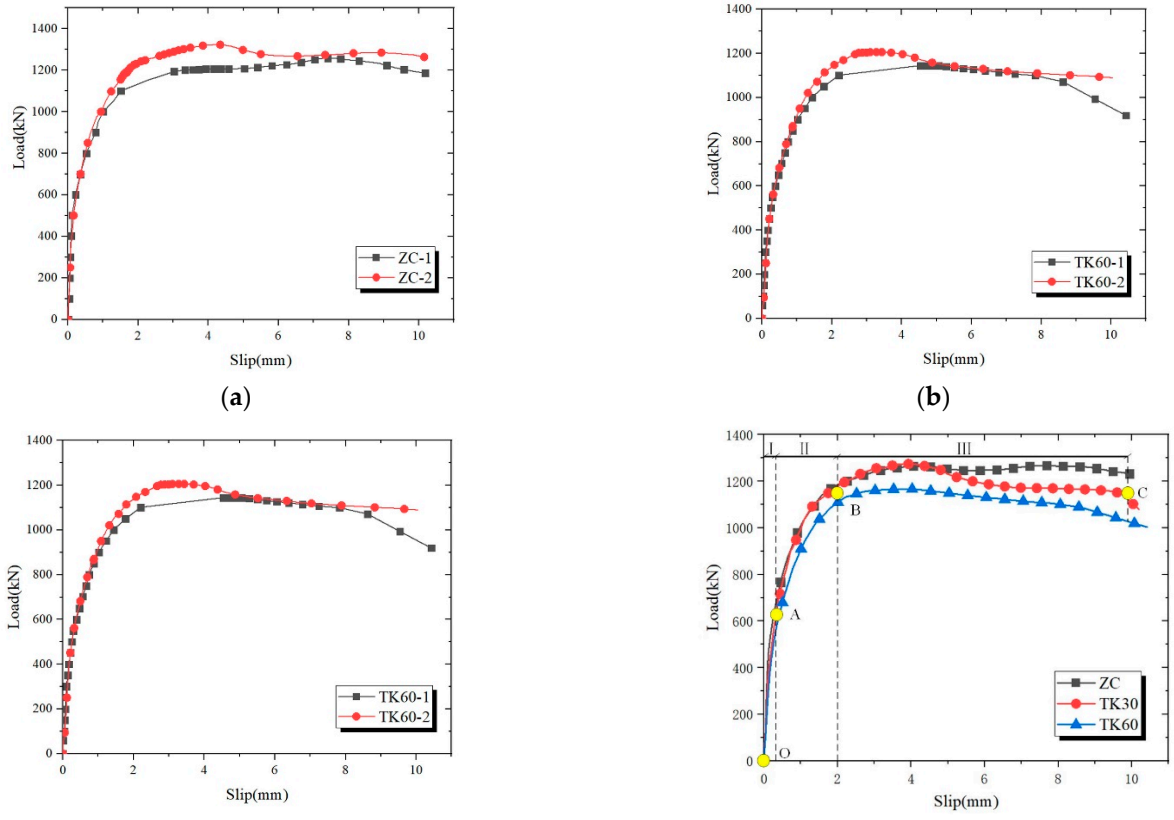

Figure 13. Load-slip curve of specimens: (**a**) ZC group; (**b**) TK30 group; (**c**) TK60 group; (**d**) Comparison of average curves. Note: I elastic stage; II elastic-plastic stage; III plastic damage stage. Yellow circles are the endpoints of each stage.

Figure 14 shows that the difference in ultimate bearing capacity of the same group of specimens is between 0.3% and 4.91%. For ZC group specimens, the failure process behavior is highly similar to TK30 and TK60 group specimens. ZC groups are given below for specific descriptions. When the specimen is in the I elastic stage, the slope of the curve is more significant, the shear stiffness is larger, the relative slip of steel–concrete is 0~0.5 mm, and the corresponding load increases up to 0.63 Pu. In the II elastic-plastic stage, there is apparent slipping at the steel-UHPC interface, the slope of the curve gradually decreases, and the load grows nonlinearly with the increase in relative slip, the slip at this stage ranges from 0.5 to 3.1 mm, and the corresponding load increases up to 0.94 Pu. In the III plastic damage stage, the load-slip curve appears to be a "platform" in this stage. The load growth is small, the relative slip increases continuously from 3.1 to 9.6 mm, and the specimen's bearing capacity decreases to about 0.95 Pu. The load-slip curves of specimens with the percentage of debonded area compared with those of naturally bonded specimens showed the same trend. There is no significant difference in the ultimate bearing capacity of specimens in the TK30 group. In contrast, the ultimate state load capacity of the specimens in the TK60 group is smaller, mainly because the degree of bonding at the steel-UHPC interface affects the force on the specimens.

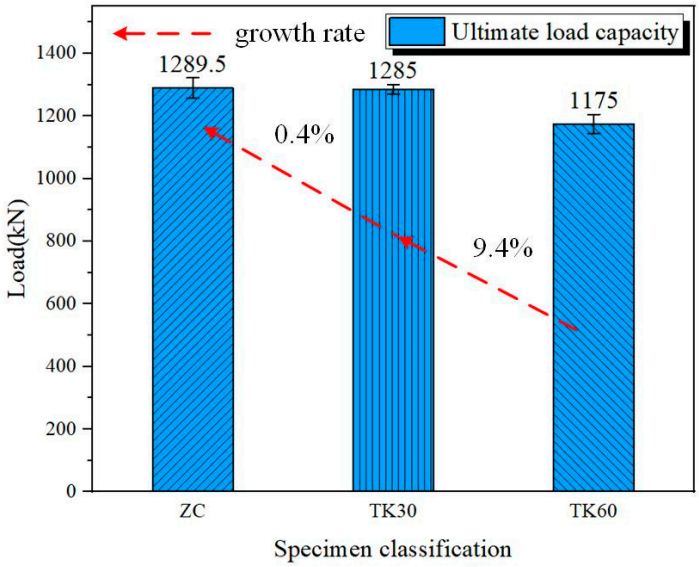

Figure 14. Comparison of ultimate shear capacity.

Figure 14 and Table 3 give the ultimate bearing capacity of each specimen. The maximum ultimate bearing capacity of the fully-bonded interface specimen is 1322 kN, the minimum is 1257 kN, and the average is 1290 kN. The maximum ultimate bearing capacity of the 30% interface defect specimen is 1301 kN, the minimum is 1269 kN, and the average is 1285 kN. The maximum ultimate bearing capacity of the 60% interface defect specimen is 1205 kN, the minimum is 1145 kN, and the average is 1175 kN. The difference in ultimate bearing capacity between naturally bonded interface specimens and 30% interface defect specimens is slight, about 0.4%. The ultimate bearing capacity of 60% interface defect specimens is 115 kN smaller than that of ZC group specimens on average, which is 9.4% lower. Therefore, it can be concluded that the ultimate bearing capacity of the full bond interface is optimal. However, the interface defects are less than 30%, and the influence on the ultimate bearing capacity can be negligible.

Table 3. Failure results of push-out tests.

Specimen	Interface Defects (%)	P_u (kN)		S_u (mm)		Failure Mode
		F	F-AVG	S	S-AVG	
ZC-1	0%	1257	1290	7.404	5.802	RF
ZC-2	0%	1322		4.200		RF
TK30-1	30%	1269	1285	3.480	4.057	RF
TK30-2	30%	1301		4.634		RF
TK60-1	60%	1145	1175	4.698	4.068	RF
TK60-2	60%	1205		3.437		RF

Note: P_u = shear capacity of the push-out specimen; S_u = interfacial slip at maximum load; RF: Fracture of shear reinforcement.

4.3. Shear Performance of PSCC Shear Connectors

4.3.1. Shear Stiffness

The shear stiffness reflects the deformation capacity of the connectors and can be used as an index to evaluate the overall performance of the bridge under the serviceability limit state. In shear connectors, the dividing point between the elastic and plastic stages of the load-slip curve is distinguished, where shear stiffness is an important criterion. However, there is no unified theoretical formula for calculating shear stiffness. Therefore, Table 4 lists the calculation methods proposed in the relevant literature to study the shear stiffness of PSCC connectors.

Table 4. Typical formulae for shear stiffness of stud connector.

Reference	Model	Notation
Eurocode 4 [27]	$k = 0.7\frac{V_{max}}{S_{0.7max}}$	V_{max} = ultimate load $S_{0.7max}$ = Slip at 0.7 times the ultimate load capacity
JSSC 1996 [31]	$k = \frac{V_{max}}{3S_{1/3max}}$	$S_{1/3max}$ = Slip at 1/3 times ultimate load capacity
Wang Y C. [32]	$k = \frac{V_{0.8}}{0.8}$	$V_{0.8}$ = Load at 0.8 mm slip
Shim C S. [33]	$k = \frac{V_{max}}{d_{sh}(0.16-0.0017f_c)}$	d_{sh} = stud diameter f_c = Concrete compressive strength (using UHPC in the article)
Lin Z F. [34]	$k = \frac{V_{0.2}}{0.2}$	$V_{0.2}$ = Load at 0.2 mm slip

According to the above five methods, the calculated shear stiffnesses of the specimens of the ZC groups, TK30 groups, and TK60 groups are shown in Table 5 and Figure 15. The stiffnesses are usually classified as elastic stiffness and elastic-plastic stiffness. The shear stiffness calculated according to the equation of EC4 is the elastic-plastic stiffness of the PSCC connector, and the discrete type of the data is within the acceptable range. The shear stiffness of the specimens with naturally bonding interfaces and the specimens with 30% interfacial defects had little effect, differing by only 0.4%. Compared with the shear stiffness of the specimens with naturally bonding interfaces, the shear stiffness of the specimens with 60% interface defects was reduced by 12%. The shear stiffness calculated according to the JSSC code is the elastic stiffness of the PSCC connector, and it is found that the discrete type is more significant for the specimens with a full bonded interface. The reason for this is that the ZC group specimens are fully bonded, and the PSCC connectors are in the elastic phase when the JSSC is calculated, mainly because the bond between steel and concrete is dominant, so the discrete type of this phase is large. In comparison, the discrete type of specimens with interface defects is lower. The shear stiffness calculated by Wang's formula is the elastic-plastic stiffness of the PSCC connector, and the dispersion of the data is lower. The shear stiffness distribution of the specimens with 30% and 60% interface defects was 1.6% and 12.8%, respectively, lower than that of the specimens with full bond interfaces. The results calculated with Shim's formula are negative, mainly because the

formula is only applicable to normal concrete and cannot be used for the calculation of UHPC specimens. The shear stiffness calculated by the Lin formula is the elastic stiffness of the PSCC connector. Therefore, the computed value of shear stiffness is higher. Compared with the shear stiffness of the specimens with naturally bonding interfaces, the shear stiffness of the specimens with 30% and 60% interface defects is reduced by 17.45% and 27.75%, respectively.

Table 5. The shear stiffness of specimens.

Calculate the Source	ZC-1	ZC-2	Average	TK30-1	TK30-2	Average	TK60-1	TK60-2	Average
EC4	1020	1119.1	1069.6	1308.5	847.6	1078.1	968.3	938.6	953.5
JSSC	4403.5	1034.8	2719.2	2663.7	2483.8	2573.8	2360.3	2262.9	2311.6
Wang	1126.0	1219.9	1173.0	1259.3	1049.9	1154.6	1031.9	1047.6	1039.8
Shim	−4.6	−4.8	−4.7	−4.6	−4.7	−4.65	−4.2	−4.4	−4.3
Lin	3005	2750	2877.5	2500	2400	2450	2250	2255	2252.5

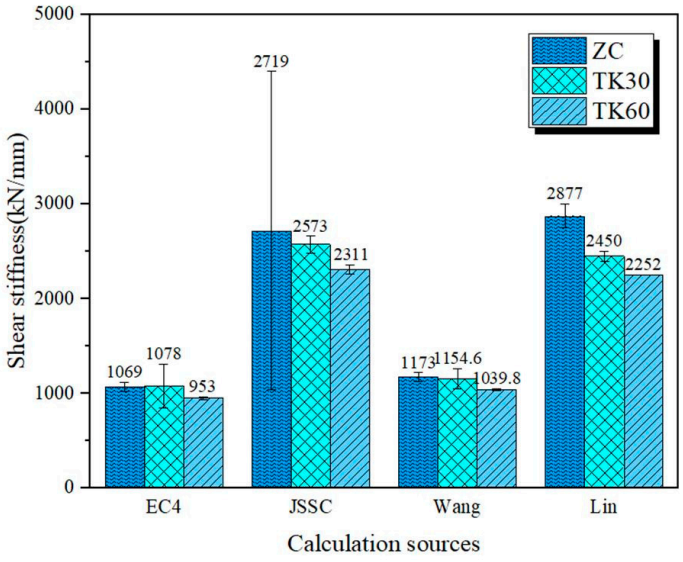

Figure 15. Comparison of shear stiffness from different calculation sources.

In conclusion, the PSCC connector is still in the working load range compared to the EC4 and Wang types. The latter discrete type is significantly lower than the former, so the Wang type is used as the shear stiffness of the PSCC in the elastic-plastic phase. Compared with the JSSC and the Lin types, both PSCC connectors are in the elastic stage. The former has a higher discrete shape in specimens with a full bonding interface, but the latter responds more stably to the shear stiffness of PSCC in the elastic phase.

By elastic stiffness and elastic-plastic stiffness analyses, specimens with naturally bonded interfaces and specimens with 30% and 60% interface defects will affect the elastic stage of stiffness. With the steel–UHPC interface bonding force enhanced, the elastic shear stiffness increased by 14.86% and 21.72%, respectively. In the elastic-plastic stage, 30% of the interfacial defects have a low effect on the elastic-plastic stiffness. However, 60% of the interfacial defects have a high effect on the elastic-plastic stiffness, which is 12.8% lower than the naturally bonded interface. The reason is that the weakening of the interfacial bond will affect the bearing capacity and ductility of the specimen, which leads to a significant reduction in the cut line stiffness.

Therefore, the compactness of the UHPC layer in the bonding cavity should be ensured during the construction phase to avoid steel-UHPC interface defects resulting in reduced shear stiffness of the PSCC connector.

4.3.2. Ductility

According to EC4 [27], the ultimate slip value S_m is the slip value corresponding to the decrease in the load to 85% of the ultimate load. The criteria for determining ductility are divided into two main methods. One is EC4, which states that a connector is considered ductile when the characteristic slip of the connector is at least 6 mm. The characteristic slip S_u is taken as the corresponding slip at the load level after a 10% decrease in ultimate load-carrying capacity.

The other is in the shear connectors structure. The ratio of the ultimate slip of the connectors to the generalized initial yield slip is defined as the ductility coefficient of the connectors, as in Equation (1). In the formula, S_e is the generalized initial yield slip, the generalized initial yield displacement of the member, also the maximum elastic deformation.

$$\mu = \frac{S_m}{S_e} \tag{1}$$

Table 6 shows that the ductility factors of all specimens are relatively large, and the characteristic slip values of all specimens S_u meet the requirements of EC4 for ductility. In EC4, it is stipulated that the shear connectors should have sufficient deformation capacity and stress redistribution in the connectors during the deformation of load. A connector with sufficient deformation capacity is a ductile connector. EC4 states that a connector can be considered ductile when the characteristic slip of the connector is at least 6 mm. In summary, the PSCC shear connector can be regarded as a ductile connector.

Table 6. Ductility of specimens.

Slip/Specimen	ZC-1	ZC-2	AVG	TK30-1	TK30-2	AVG	TK60-1	TK60-2	AVG
S_m (mm)	11.42	10.32	10.87	10.18	10.19	10.19	9.74	10.11	9.93
S_u (mm)	11.22	10.68	10.95	9.46	9.54	9.50	7.52	10.03	8.78
S_e (mm)	1.73	1.51	1.62	1.66	1.93	1.80	1.77	1.82	1.80
Ultimate ductility ratio (μ)	6.60	6.83	6.72	6.13	5.60	5.87	5.50	5.24	5.37

In addition, for the ductility coefficients of the specimens, all groups of specimens meet the requirement of ductility coefficients to be more significant than 5. The ductility coefficients of specimens with 30% and 60% interfacial defects are reduced by 12.6% and 20.1%, respectively, compared with the specimens with naturally bonded interfaces. Therefore, the interfacial bonding force affects the ductility of the specimens to some extent. Thus, inadequate pouring of UHPC should be avoided in the project, leading to the effect of interface defects.

4.4. Comparison with Test Data in the Literature

To further analyze the ultimate load-bearing capacity, shear stiffness, and ductility of PSCC shear connectors, the ZC group with full bonds at the interface and TK30 and TK60 groups with defective interface bonds were compared with the push-out test results of the stud connectors with UHPC as concrete material in the literature [23,26,35]. The failure mode of all specimens in this paper is shear reinforcement shear failure, but all specimens in the listed literature are stud shear failure. To eliminate the effect of stud strength in different tests, the results of dividing the ultimate load capacity P_u of the specimen by the product of the cross-sectional area A_s of all stud/shear reinforcement studs and the yield strength f_s of the stud/shear reinforcement are compared.

Table 7 summarizes the results and failure patterns of the tests with different diameter stud connectors from the literature. Compared with the specimens with the same stud diameter, the bearing capacity of the PSCC connector was increased by 1.93 times compared with PS13. The difference in bearing capacity was minor compared with the modified stud connector of Guo et al. The load carrying capacity of the PSCC connector was increased by 100% compared to the specimen with a stud diameter of 19 mm and by 10% compared to

the load carrying capacity of the modified stud connector of Zou et al. After normalization, the shear bearing capacity of the PSCC connector was improved by 7.14 times and 8.5 times compared with the conventional stud connector of 13 mm and 16 mm, respectively.

Table 7. Comparison of the shear resistance of stud connectors in different literature.

Specimen	D (mm)	P_u (kN)	$\frac{P_u}{A_s f_s}$	S_u (mm)	S_m (mm)	$k_{0.2}$ (kN/mm)	Failure Mode
ZC-1	12	1257	1.67	7.40	11.42	3005	RF
ZC-2	12	1322	1.76	4.20	10.32	2750	RF
Average	-	1290	1.71	5.8	10.87	2877.5	-
TK30-1	12	1269	1.69	3.48	10.18	2500	RF
TK30-2	12	1301	1.73	4.63	10.19	2400	RF
Average	-	1285	1.71	4.06	10.19	2450	-
TK60-1	12	1145	1.52	4.70	9.74	2250	RF
TK60-2	12	1205	1.60	3.44	10.11	2255	RF
Average	-	1175	1.56	4.07	9.93	2252.5	-
PS13-1 [23]	13	436	0.21	2.45	3.38	272.2	SF
PS13-2	13	445	0.21	1.48	3.42	278.1	SF
Average	-	441	0.21	1.87	3.40	275.2	-
PS19-1	19	537	0.18	3.27	6.07	335.3	SF
PS19-2	19	750	0.17	3.38	4.64	468.4	SF
Average	-	644	0.18	3.33	5.36	401.9	-
PS-1 [26]	16	1199	1.16	7.81	9.63	304.9	SF
PS-2	16	1144	1.10	4.96	7.77	218.1	SF
PS-3	16	1156	1.11	7.81	9.82	214.5	SF
Average	-	1166	1.12	6.86	9.07	245.8	-
PR-1	16	1242	1.20	6.10	11.47	300	SF
PR-2	16	1268	1.22	4.80	8.55	250.8	SF
PR-3	16	1212	1.17	5.87	9.10	292.4	SF
Average	-	1241	1.20	5.59	9.71	281.1	-
M1R1H1-1 [35]	13	1427	2.08	2.68	5.32	2495	SF
M1R1H1-2	13	1547	2.26	4.21	5.00	3856	SF
Average	-	1487	2.17	3.45	5.16	3176	-
M1R2H1-1	13	1366	1.99	3.30	7.79	2883	SF
M1R2H1-2	13	1409	2.06	2.77	3.98	3484	SF
Average	-	1388	2.03	3.04	5.89	3184	-

Note: D = Diameter of the stud/the reinforcement P_u = shear capacity of the push-out specimen; S_u = interfacial slip at ultimate load; S_m = interfacial slip at 85% ultimate load; $k_{0.2}$ = Slope of cut line at 0.2 mm; RF: Fracture of shear reinforcement; SF: Fracture of a stud.

The PSCC connectors had higher ductility than the specimens with stud fracture despite the failure mode of shear reinforcement fracture. Although the difference in the slip S_u under ultimate load was not significant for each specimen, the ultimate slip S_m of PSCC connectors is 2.2 times and 100% higher than that of conventional stud connectors with diameters of 13 mm and 19 mm, respectively. The ultimate slip S_m of the PSCC connectors was 19.85% and 84.55% higher than the ultimate slip S_m of the modified stud connectors of Zou et al. and Guo et al., respectively. In terms of elastic stiffness, the PSCC connectors differed less from those of Guo et al. but were much improved over conventional connectors.

In summary, PSCC connectors demonstrate improved shear performance by comparing the load-bearing capacity, ductility, and stiffness with conventional stud connectors. Furthermore, the original purpose of PSCC connectors is not to surpass traditional connectors in shear performance but to highlight the ease of construction for assembled construction and meeting the shear performance of conventional stud connectors.

5. Finite Element Analysis

5.1. General

In this paper, the finite element software ABAQUS was used to simulate the test. Because of the symmetry of the test specimens, a 1/4 model was established to save computational time. The model shown in Figure 16 was divided into six parts: steel plate, concrete, studs, shear connection steel member, structural reinforcement, and UHPC. Except for the structural reinforcement, which was simulated by the B31 beam unit, all the other parts were simulated by the C3D8 3D eight-node unit. The overall unit size is 12 mm, while the unit size for studs and shear connection steel members is refined to 5 mm.

The interaction between studs and UHPC, the interaction between shear connected steel members and UHPC, and the interaction between shear connected steel members and normal concrete were performed using normal hard contact and tangential penalty functions with friction coefficients of 0.9, 0.7, and 0.6, respectively. In addition, the structural reinforcements were embedded in the concrete.

As shown in Figure 16, 3D translation and rotation constraints were applied to the bottom surface of the prefabricated plate with direction n. The main purpose was to simulate the foundation. In the test, the steel box and the stud were welded together so that the two were combined into a single member in the model without any further constraints being applied. Due to the symmetry of the model, a symmetric surface restraint was used on the steel members and the concrete slab. The model took displacement loading, coupling the top surface of the loaded steel plate with the reference point RP2, and the displacement loading was applied to the reference point RP2. To avoid loading fluctuation, the amplitude of reference point RP2 was set to 20 mm with smooth amplitude.

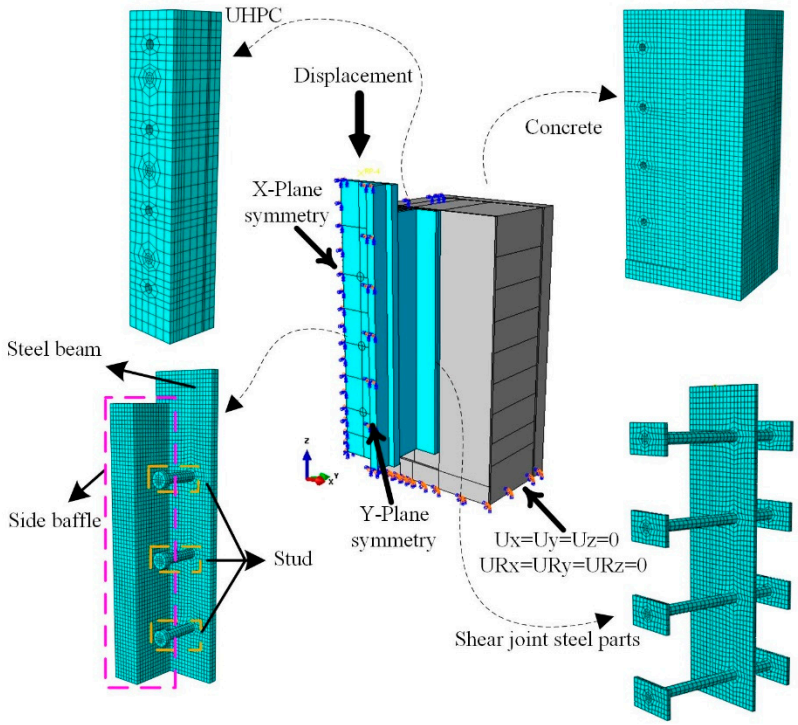

Figure 16. Modeling and boundary conditions.

5.2. Material Models

(1) Material Constitution Model of UHPC

The UHPC constitutive model used in the numerical model was derived from the tensile model proposed by Zhang et al. [36]. The compressive model was proposed by Yang et al. [37]. As shown in Figure 17, the material parameters are shown in Table 8. The Poisson's ratio of UHPC is 0.2.

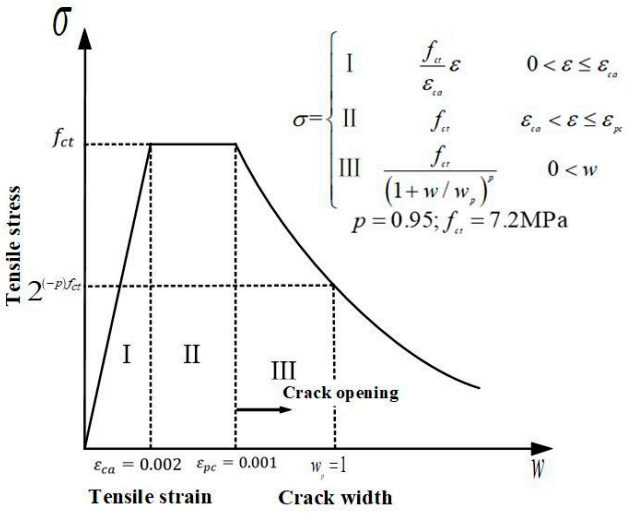

(**a**)

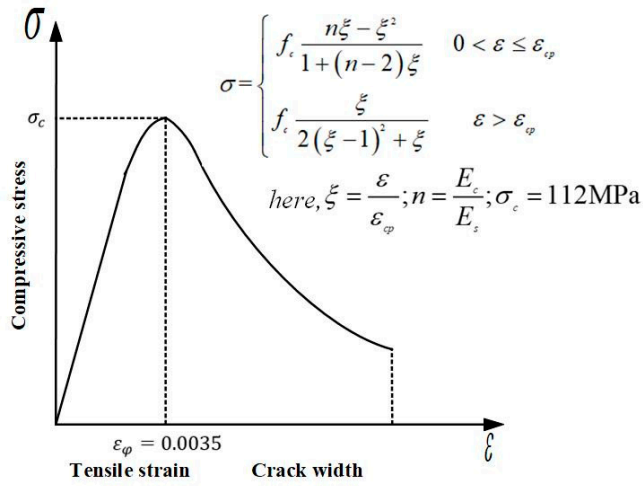

(**b**)

Figure 17. Constitutive relationship of the UHPC: (**a**) Tensile stress-strain relationship. (**b**) Tensile stress-strain relationship.

Table 8. UHPC material parameters.

Expansion Angle (Ψ)	Eccentricity (λ)	Yield Stress Ratio $\frac{\sigma_{bo}}{\sigma_{c0}}$	Invariant Stress Ratio K_c	Coefficient of Viscosity
36°	0.1	1.16	0.6667	0.0005

(2) Material constitution model of steel plates and structural reinforcement

For this model, the steel was selected from the ideal elastic-plastic model, and the elastic modulus, yield strength, and ultimate strength were taken according to the material test results. The type of steel used in the model is HRB400, whose standard value of yield strength is f_{sk} = 400 MPa, the elastic modulus is $E_s = 2.0 \times 10^5$ MPa, Poisson's ratio is 0.2, and the constitutive relationship is depicted in Figure 18.

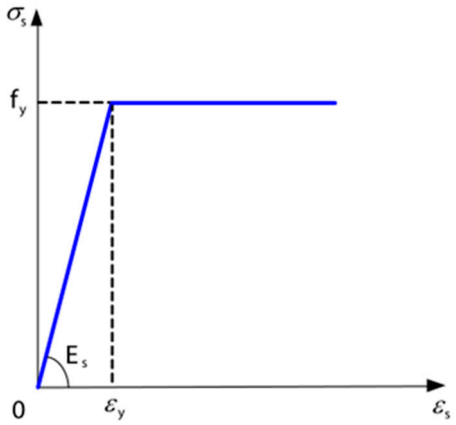

Figure 18. Constitutive relationship between the steel and structural reinforcement.

(3) Material constitution model of studs and shear reinforcement

In the push-out test, the box steel type member was still in the elastic phase when the shear connection member was damaged, but the stud or shear reinforcement had gone through the elastic-plastic phase until fracture and damage. Therefore, in the finite element simulation, both take a trifold model, as shown in Figure 19, to reduce the stress of the material after it reaches the ultimate strain to simulate its exit from work.

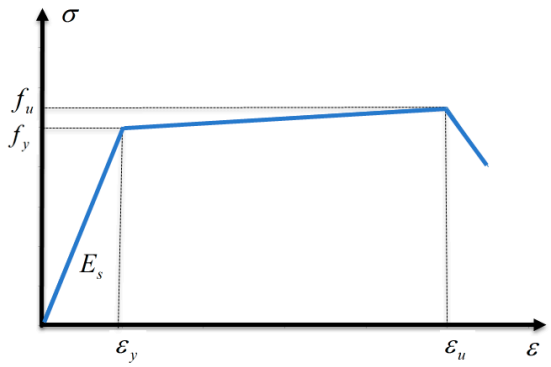

Figure 19. Constitutive relationship of the stud and shear reinforcement.

(4) Material constitution model of concrete

For the precast slab part of the model, the concrete damaged plasticity model [38] provided by ABAQUS was used, which includes concrete compression damage and tensile damage. The parameters of the model are shown in Table 9. In the damage model, a damage factor D is introduced to represent the stiffness degradation of concrete in tension and compression. The value of D ranges from 0 to 1, where 0 indicating no damage and 1 indicating complete material stiffness degradation. The stress-strain relationship curves of the concrete and the tensile stress-strain curve are presented in Figure 20. The concrete material parameters are shown in Table 9.

Table 9. Concrete material parameters.

Material	Expansion Angle	Eccentricity	The Ratio of Axial Compression Stress to Strength	Yield Constant	Coefficient of Viscosity
C50	37°	0.1	1.16	0.6667	0.0005

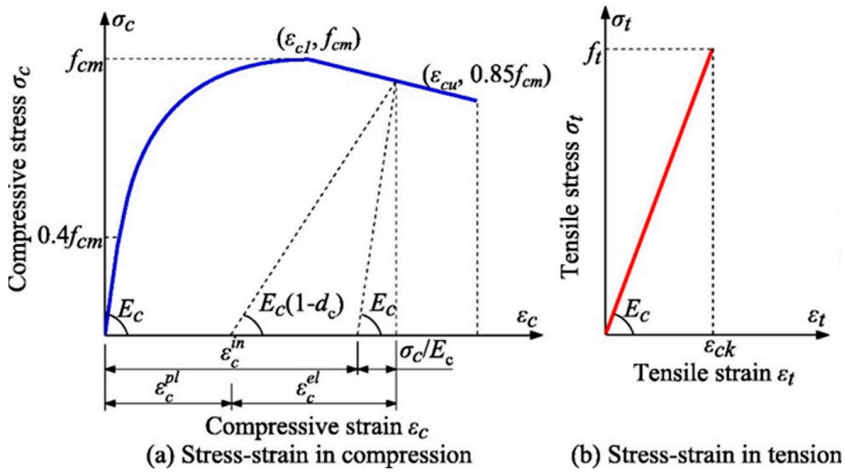

Figure 20. Material constitution of concrete.

5.3. Validation of Numerical Simulation Model

5.3.1. Validation of Load-Slip Curves

A comparison of the load-slip curves of the finite element model results for the PSCC connectors and the load-slip curves of the test results for the PSCC connectors is shown in Figure 21. It can be seen that the established finite element model can simulate the whole process of the PSCC connector well, which is mainly divided into three stages: elastic stage, plastic stage, and plastic damage stage. Compared with the push-out test, the error range of the ultimate shear bearing capacity of the PSCC connector simulated by the finite element is within 4%. The load-slip curves in the finite element have the same trend as that in the test, thus indicating that the finite element is similar to the test results.

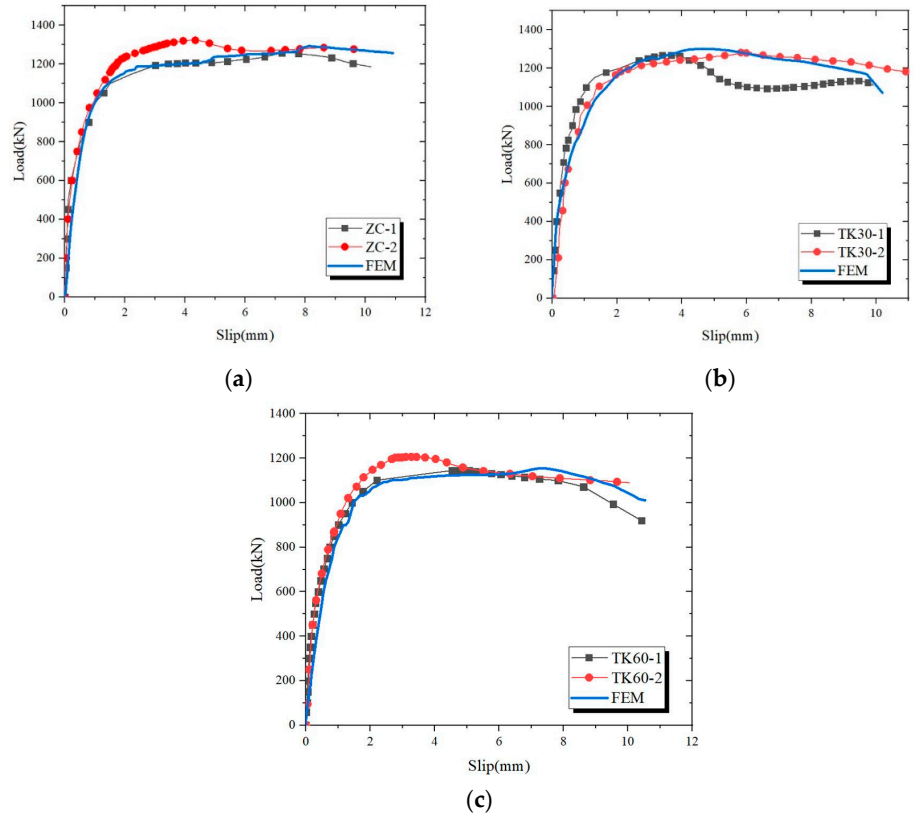

Figure 21. Comparison of load-slip curves from tests and FE analysis: (**a**) ZC group; (**b**) TK30 group; (**c**) TK60 group.

5.3.2. Failure Process Analysis

Since the three groups of specimens had the same failure mode, the ZC group specimens were used as a representative for the analysis. Figure 22 shows the failure mode in the finite element simulation of the PSCC connector compared to that in the push-out test. Figure 23 shows that in the elastic stage, slight local damage is observed at the UHPC around the root of the bottom shear reinforcement in the bonding cavity. The stresses of the shear reinforcement and studs are lower than the yield strength. In the elastic-plastic stage, the damage of the UHPC at the root of the shear reinforcement increases gradually as the load increases, the stress of the bottom shear reinforcement reaches yield, and there is no significant stress at the root of the studs. In the plastic stage, the stress in the shear reinforcement in the bonding cavity reaches an ultimate strength of 580 MPa. Shear reinforcement gradually fractures from the bottom to the top, and the UHPC layer damage gradually expands from around the shear reinforcement, resulting in complete failure of the adhesion between the sealing steel plate and the UHPC interface. However, there is no large deformation at the root of the stud. Therefore, the interfacial bond between the steel box and the UHPC interface is significantly better than that between the sealing steel plate and the UHPC interface. The overall crack distribution of the concrete slab in the finite element model of each group of specimens under the ultimate condition is consistent with that observed during the test. Based on the above analysis, the finite element model established in this paper for pushing and squeezing tests can better simulate the shear behavior and final failure mode of PSCC connectors.

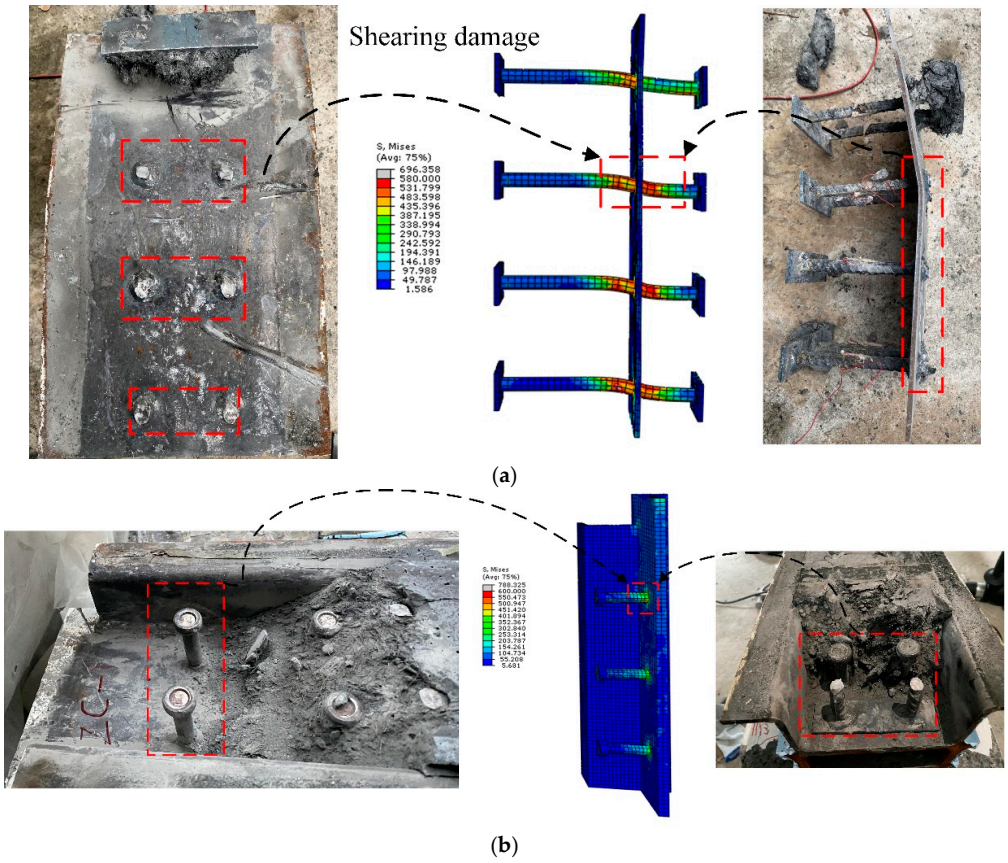

Figure 22. *Cont.*

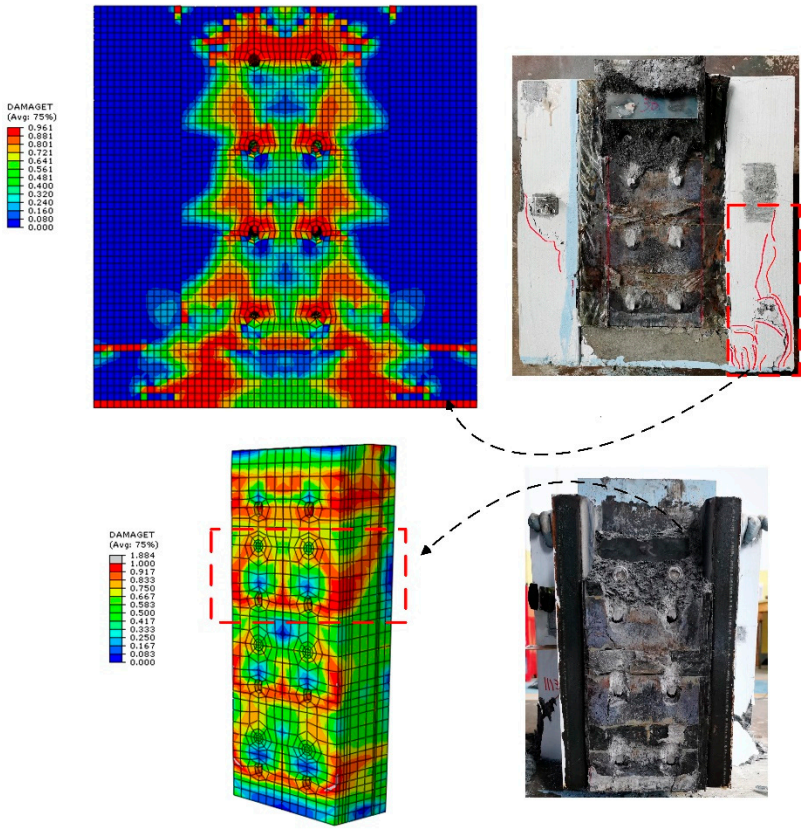

(**c**)

Figure 22. The failure mode of FEM simulation and test: (**a**) Shear reinforcement; (**b**) Stud; (**c**) Concrete and UHPC.

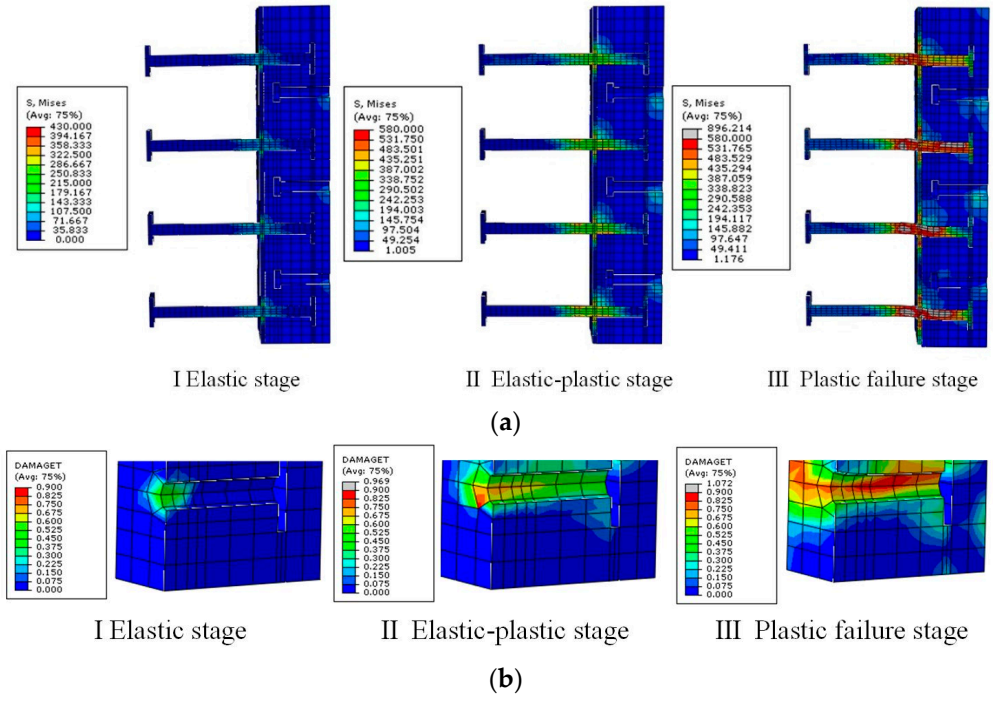

Figure 23. Variation of concrete damage and Shear reinforcement stress during the loading: (**a**) Shear reinforcement and stud; (**b**) UHPC.

5.4. Parametric Studies

5.4.1. Diameter of Shear Reinforcement

According to the results of this push-out test, when the shear strength ratio of shear reinforcement to the stud is 1.09, the failure mode of the PSCC connector exhibits the shear failure of the shear reinforcement. To investigate another failure mode of PSCC connectors, the shear strength ratio of the shear reinforcement to the stud is increased by increasing the cross-sectional area of the shear reinforcement, which eventually leads to the shear failure of the stud. The final failure mode was determined by varying the shear strength ratio (Figure 24). Therefore, based on the experimental design and with the material strength kept constant, the shear reinforcement diameter was increased from the initial 12 mm to 14 mm and 16 mm to analyze the mechanical properties of the PSCC connectors at different section ratios.

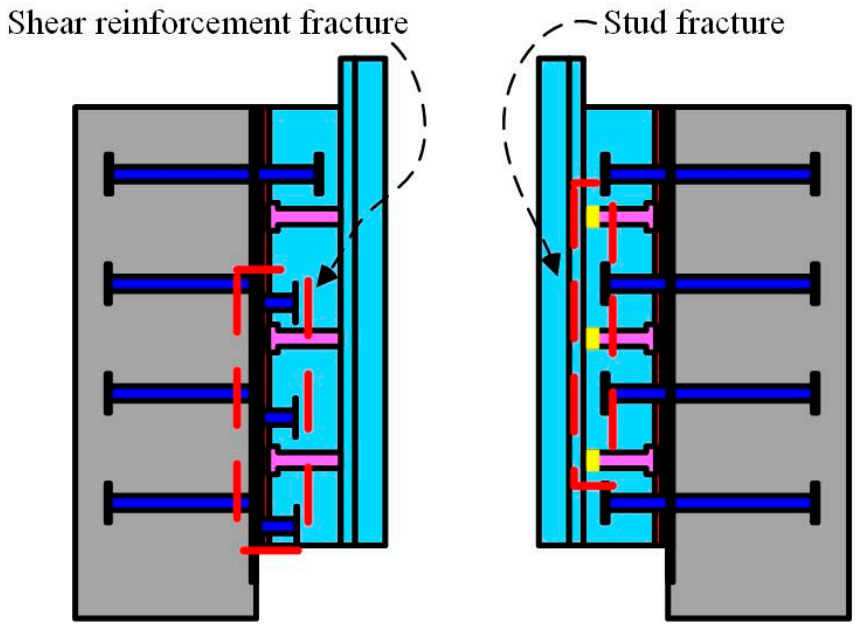

Figure 24. Two types of failure forms.

Figure 25 and Table 10 show that the load-slip curves of specimens with different shear reinforcement diameters are divided into three stages: elastic, plastic, and damage stages. The bearing capacity of the specimens increases gradually with the increase in shear reinforcement diameter. In Table 11, the effect of shear reinforcement diameter on the shear bearing capacity (P_u), elastic stiffness ($k_{0.2}$), and the slip of a single stud in PSCC connectors is shown. The finite element results show that the ultimate shear bearing capacity of the PSCC connection increases by 18.8% and 9.3%, and the shear strength of the PSCC connection increases by 13.1% and 4.8% as the cross-sectional area of shear reinforcement increases by 36% and 78%, respectively. Thus, shear reinforcement diameter and shear resistance of PSCC connectors are positively correlated, but the growth rate decreases with increasing reinforcement diameter. This is because the shear reinforcement shear strength reaches a specific value, and the main object to control the shear performance changes to studs.

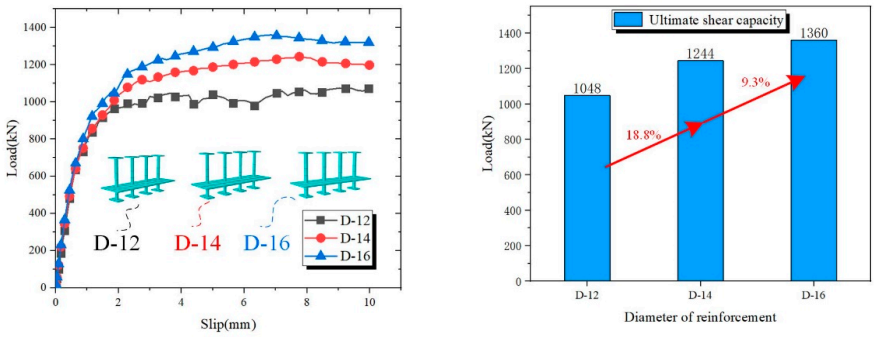

(**a**) (**b**)

Figure 25. Analysis results for reinforcement diameters:(**a**) Load-slip curves; (**b**) Comparison of ultimate shear capacity.

Table 10. Comparison of FEM and experiment.

Specimen Classification	P_u	FEM	P_u	Deviation	Failure Mode
ZC-1	1257	ZC-FEM	1285	2.2%	RF
ZC-2	1322			2.8%	
TK30-1	1269	TK30-FEM	1284	1.2%	RF
TK30-2	1301			1.3%	
TK60-1	1145	TK60-FEM	1155	0.9%	RF
TK60-2	1205			4.1%	

Note: P_u = shear capacity of the push-out specimen; S_u = interfacial slip at maximum load; S_m = Ultimate slip value; RF: Fracture of shear reinforcement.

Table 11. Analysis of shear stiffness at different diameters.

Diameter of Reinforcement (mm)	$P_{0.2}$ (kN)	P_u (kN)	$k_{0.2}$ (kN/mm)	$k_{0.8}$ (kN/mm)
D-12	221	1048	1105	978
D-14	250	1244	1250	755
D-16	262	1360	1310	809

Note: $P_{0.2}$ = load at 0.2 mm slip; P_u = shear capacity of the push-out specimen; $k_{0.2}$ = Slope of cut line at 0.2 mm; $k_{0.8}$ = Slope of cut line at 0.8 mm.

In Figure 26, the strain at the root of the reinforcement pre-embedded in the UHPC gradually decreases as the diameter of the shear reinforcement increases, and the strain at the root of the stud gradually increases. When the shear reinforcement diameter is 16 mm, the failure mode of the PSCC connection is stud shear failure. The results show that when the material properties are the same, the ratio of shear reinforcement to stud section is 1.55. The failure characteristics of PSCC connectors show stud shear failure.

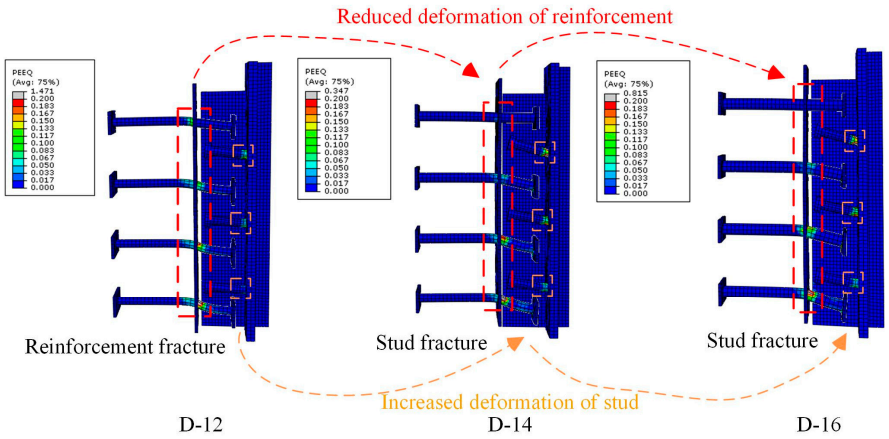

Figure 26. Damage results of studs and shear reinforcement.

5.4.2. Shear Reinforcement and Stud Spacing

In practical engineering, reducing the UHPC used in the connection layer can make the bridge weight lower, which helps meet the design requirements and also improves economic efficiency. Therefore, to obtain the optimal width of the connection layer, a parametric analysis was carried out to analyze the effect of the spacing change between the center of the studs and the center of shear reinforcement on the mechanical properties. A total of three groups of spacing were analyzed for 3d, 4d, and 5d, and the specific arrangement is shown in Figure 27.

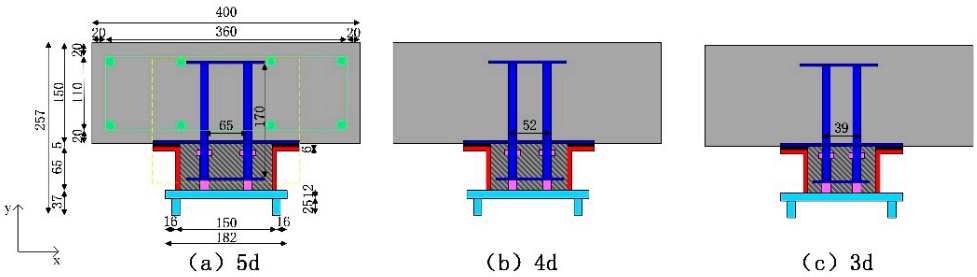

Figure 27. Spacing arrangement of shear reinforcement and studs.

According to the test results, when the stud spacing is 5d, the PSCC connector has a high load capacity and good ductility. Therefore, when the spacing of the studs is 5d, the PSCC connectors meet the requirements of shear resistance. In Figure 28, according to the finite element analysis, there is no change in the damage mode when the spacing of studs and shear reinforcement is reduced to 3d and 4d. The ultimate load-carrying capacity with a spacing of 5d increased by 11.17% compared to that with a spacing of 4d. The ultimate bearing capacity of the spacing of 4d increased by 7.23% compared to that of 3d. This shows that the maximum shear bearing capacity of the specimens is significantly reduced after the spacing is reduced. Nevertheless, the PSCC connectors still have good ductility after the spacing is reduced and meets the relevant requirements in EC4.

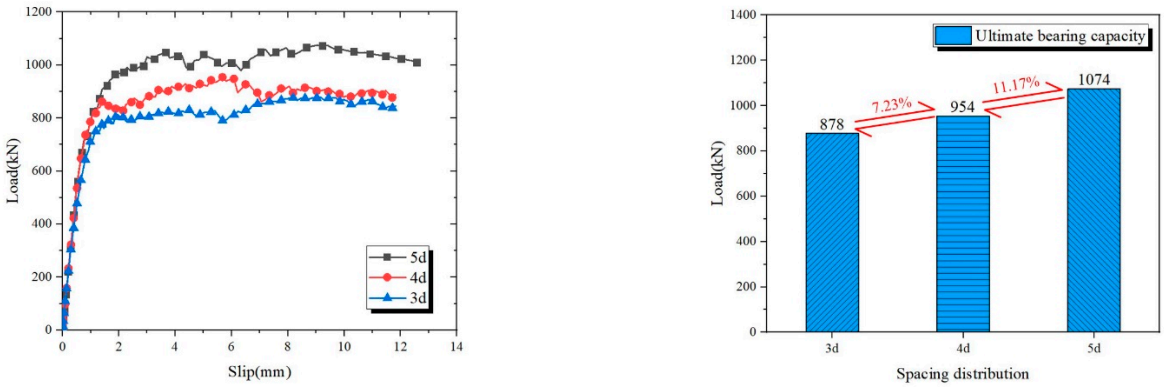

Figure 28. Analysis results of spacing arrangement: (**a**) Load-slip curves; (**b**) Comparison of ultimate shear capacity.

Figure 29 shows the Mises stress distribution of each component with different spacing. As the spacing increases, the damage of the precast slab gradually expands at the middle of the second and third rows of shear reinforcement. The reason is that as the spacing increases, the amount of UHPC increases, and the restraint on the shear reinforcement increases, thus the internal force transferred to the precast slab increases. Since the ends of the shear reinforcement are well restrained, the shear reinforcement has to be deformed, thus causing concrete damage on both sides. Since the strength and stiffness of UHPC are more significant than the strength and stiffness of precast concrete, the precast concrete

is crushed. When the spacing is reduced to 3d, the amount of UHPC is reduced, but the restraint of UHPC on the shear reinforcement is weakened, so the deformation of the shear reinforcement buried in the bonding cavity is relatively large.

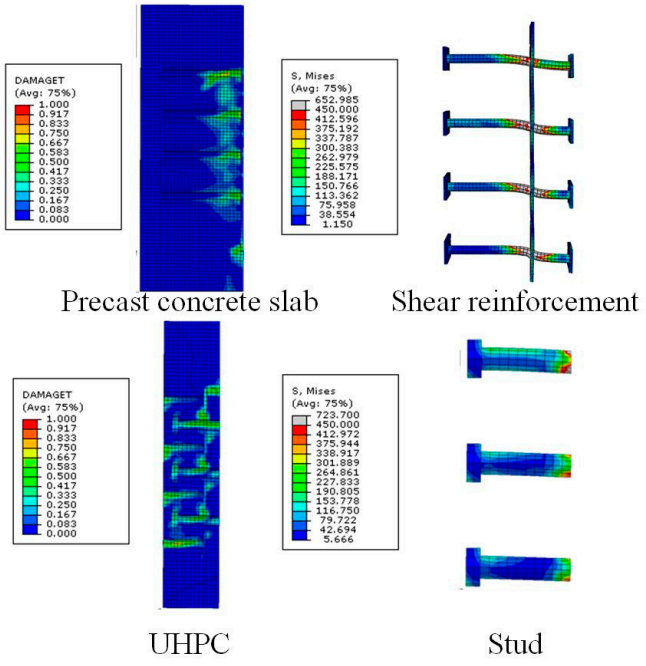

(**a**)

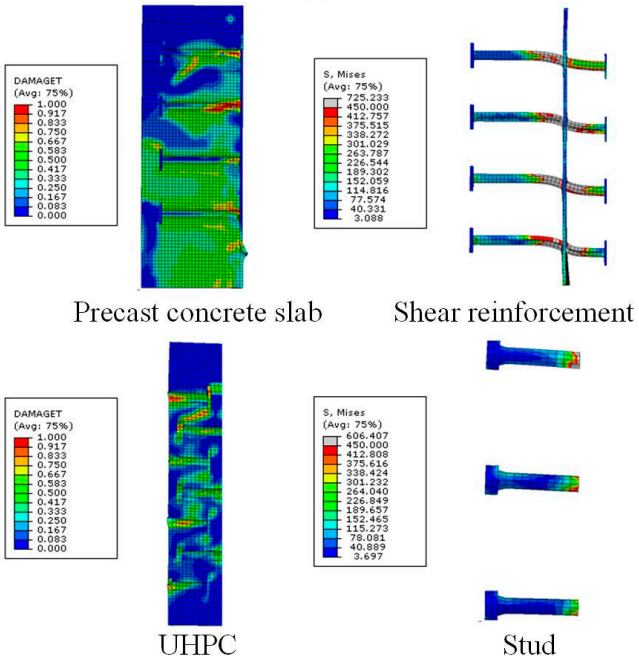

(**b**)

Figure 29. *Cont.*

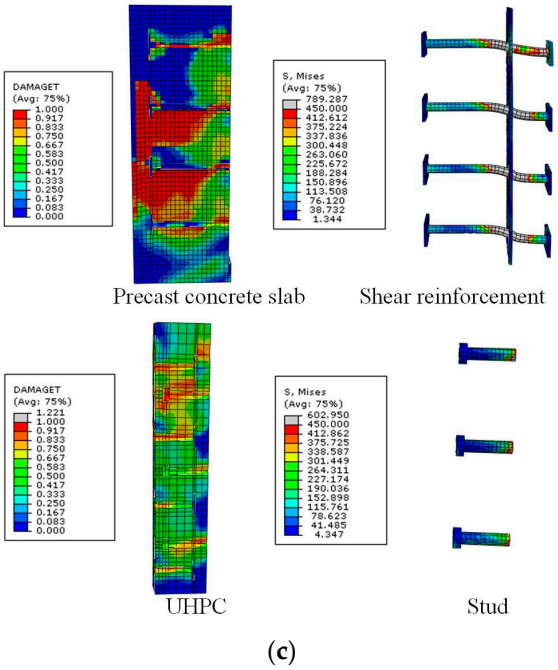

(**c**)

Figure 29. Mises stress distribution: (**a**) 3d; (**b**) 4d; (**c**) 5d.

In summary, although the amount of UHPC can be minimized when the spacing is located at 3d, the ultimate bearing capacity of the PSCC connector is reduced by 22.3%, and the deformation of shear reinforcement is more significant. While the spacing is at 4d, PSCC can maintain a higher ultimate bearing capacity while the deformation of shear reinforcement is closer to that at 5d. Therefore, 4d is chosen as the optimal spacing between studs and shear reinforcement.

6. Conclusions

To study the shear performance of PSCC shear connectors, this paper conducted an experimental study of PSCC connectors at the steel-UHPC interface using both full bonds and the percentage of debonded area as the main parameters. The failure modes, load-slip curves, shear stiffness and ductility of the specimens were analyzed based on the test results. In addition, the reliability of the numerical model of the PSCC connectors was verified by the test results. Therefore, a parametric analysis was performed based on the diameter and spacing of the studs and shear reinforcement. The main conclusions are summarized as follows:

(1) The failure mode of PSCC depends on the shear strength ratio of the studs to the shear reinforcement. When the shear strength ratio of shear reinforcement to studs is 1.09, the failure mode of the test is shear damage of shear reinforcement. In addition, the failure mode of PSCC connectors is not affected by the percentage of debonded area.

(2) The average shear capacity of PSCC connectors increases as the percentage of debonded area decreases. The average shear capacity of the specimen with 30% debonded area rate reduces by 0.4% compared to the average capacity of the naturally bonding interface specimen. The average shear capacity of the specimen with 60% debonded area rate reduces by 9%. In addition, PSCC shear connectors have high ductility and meet the characteristic slip value of more than 6 mm under EC4 specification under different parameters, so PSCC connectors can be considered ductile connectors.

(3) The interfacial defect has a large effect on the elastic stiffness but a small effect on the elastic-plastic stiffness since the interfacial bond fails after the elastic stage. The elastic stiffness of the specimens with 30% debonded area and the specimens with 60% debonded area decreased by 14.8% and 21.7%, respectively, compared with the specimens with a naturally bonded interface. Although the 30% debonded area

rate has a negligible effect on the shear performance of PSCC connectors, the underpouring of UHPC should be avoided during the construction process.

(4) A parametric analysis was performed based on a modified finite element model, which was experimentally validated. The boundaries of two types of failure modes of PSCC connectors were clarified. By finite element parameter analysis, when the ratio of shear reinforcement to stud cross-section is less than 1.55 times, the failure mode is the shear failure of shear reinforcement. On the contrary, the failure mode is the shear failure of studs.

(5) The transverse spacing between the stud and the shear reinforcement was studied to obtain the optimal bonding cavity width to meet the design requirements and improve economic efficiency. After the spacing was increased from 3d to 4d and 5d, the PSCC ultimate bearing capacity was increased by 7.23% and 22.3%, respectively, and the deformation of shear reinforcement in the bonding cavity was significantly reduced. However, the precast plate damage was gradually extended. Therefore, when the transverse spacing of both studs and shear reinforcement is 4d, the shear performance can be guaranteed in PSCC connectors.

Author Contributions: F.Z. proposed the concept of research, developed research methods, conducted experiments and data analysis, and wrote and prepared the original draft. C.G., J.G. and J.Z. reviewed and edited the manuscript, supervised the study, were in charge of the project administration, and acquired the funding. J.J. and L.N. conducted data curation. All authors have read and agreed to the published version of the manuscript.

Funding: This research was funded by Major Science and Technology Projects in Hainan (ZDKJ2021048), the National Natural Science Foundation of China (52008066), Science and technology projects in T.A.R. (XZ202001ZY0054G), National Natural Science Foundation of China (52278147), and National Natural Science Foundation of China (52208302).

Institutional Review Board Statement: Not applicable.

Informed Consent Statement: Not applicable.

Data Availability Statement: The data presented in this study are available upon reasonable request from the corresponding author.

Conflicts of Interest: The authors declare no conflict of interest.

References

1. Wang, Y.H.; Yu, J.; Liu, J.P.; Chen, Y.F. Shear behavior of shear stud groups in precast concrete decks. *Eng. Struct.* **2019**, *187*, 73–84. [CrossRef]
2. Kruszewski, D.; Wille, K.; Zaghi, A.E. Push-out behavior of headed shear studs welded on thin plates and embedded in UHPC. *Eng Struct.* **2018**, *173*, 429–441. [CrossRef]
3. Leblouba, M.; Barakat, S.; Ahmed, M.S.; Al-Toubat, S. Shear strength at the interface of precast bridge concrete decks and girders subjected to cyclic loading with varying speeds. *Eng Struct.* **2019**, *196*, 109296. [CrossRef]
4. Culmo, M.P.; Lord, B.; Huie, M.; Beerman, B. *Accelerated Bridge Construction—Experience in Design, Fabrication and Erection of Prefabricated Bridge Elements and Systems*; Federal Highway Administration: Washington, DC, USA, 2011.
5. Shahawy, M. *Prefabricated Bridge Elements and Systems to Limit Traffic Disruption during Construction*; Nchrp Synthesis of Highway Practice. Transportation Research Board: Washington, DC, USA, 2003.
6. Sprinkel, M. *Prefabricated Bridge Elements and Systems*; Nchrp Synthesis of Highway Practice: Washington, DC, USA, 1985; Volume 119.
7. Zona, A.; Ranzi, G. Shear connection slip demand in composite steel-concrete beams with solid slabs. *J. Constr. Steel Res.* **2014**, *102*, 266–281. [CrossRef]
8. Zhuang, B.; Liu, Y.; Yang, F. Experimental and numerical study on deformation performance of Rubber-Sleeved Stud connector under cyclic load. *Constr. Build. Mater.* **2018**, *192*, 179–193. [CrossRef]
9. Zhuang, B.; Liu, Y. Study on the composite mechanism of large Rubber-Sleeved Stud connector. *Constr. Build. Mater.* **2019**, *211*, 869–884. [CrossRef]
10. Oguejiofor, E.C.; Hosain, M.U. A parametric study of perfobond rib shear connectors. *Can. J. Civil. Eng.* **1994**, *21*, 614–625. [CrossRef]
11. Yang, H.L.; Zheng, Y.; Mo, S.X.; Lin, P.H. Push-out tests on studs with UHPC cover embedded in UHPC-NSC composite slab. *Constr. Build. Mater.* **2022**, *331*, 127210. [CrossRef]

12. Xu, X.; Liu, Y. Analytical and numerical study of the shear stiffness of rubber-sleeved stud. *J. Constr. Steel Res.* **2016**, *123*, 68–78. [CrossRef]
13. Chen, X.; Sugiura, K.; Chong, W. Parametrical static analysis on group studs with typical push-out tests. *J. Constr. Steel Res.* **2012**, *72*, 84–96.
14. He, Y.L.; Guo, S.J.; Wang, L.C.; Yang, Y.; Xiang, Y.Q. Experimental and numerical analysis of grouped stud shear connectors embedded in HFRC. *Constr. Build. Mater.* **2020**, *242*, 118–197.
15. Tan, C.; Zhang, Y.; Zhao, H.; Zhang, B.; Du, T. Study on Shear-Lag Effect of Steel–UHPC Ribbed Slab Composite Structures Using Bar Simulation Method. *Buildings* **2022**, *12*, 1884. [CrossRef]
16. Zhang, Z.G.; Yang, F.; Liu, J.; Wang, S.P. Eco-friendly high strength, high ductility engineered cementitious composites (ECC) with substitution of fly ash by rice husk ash. *Cem. Concr. Res.* **2020**, *137*, 106200. [CrossRef]
17. Ahmed, S. Enhancement of Ultrahigh Performance Concrete Material Properties with Carbon Nanofiber. *Adv. Civ. Eng.* **2014**, *2014*, 854729. [CrossRef]
18. Xiang, S.; Gao, Y. Synthesis of Pectiniform Polyurethane-Modified Polycarboxylate and Its Preliminary Application in Ultrahigh-Performance Concrete. *Adv. Civ. Eng.* **2020**, *2020*, 8859093. [CrossRef]
19. Zou, Y.; Zheng, K.D.; Zhou, Z.X.; Zhang, Z.Y.; Guo, J.C.; Jang, J.L. Experimental study on flexural behavior of hollow steel-UHPC composite bridge deck. *Eng. Struct.* **2023**, *274*, 115087. [CrossRef]
20. Wang, Z.; Nie, X.; Fan, J.S.; Lu, X.Y.; Ding, R. Experimental and numerical investigation of the interfacial properties of non-steam-cured UHPC-steel composite beams. *Constr. Build. Mater.* **2019**, *195*, 323–339. [CrossRef]
21. Luo, J.; Shao, X.; Fan, W.; Cao, J.; Deng, S. Flexural cracking behavior and crack width predictions of composite (steel + UHPC) lightweight deck system. *Eng. Struct.* **2019**, *194*, 120–137. [CrossRef]
22. Fang, Z.C.; Liang, W.B.; Fang, H.Z.; Jiang, H.B.; Wang, S.D. Experimental investigation on shear behavior of high-strength friction-grip bolt shear connectors in steel-precast UHPC composite structures subjected to static loading. *Eng. Struct.* **2021**, *244*, 112777. [CrossRef]
23. Tong, L.; Chen, L.; Wen, M.; Xu, C. Static behavior of stud shear connectors in high-strength-steel–UHPC composite beams. *Eng. Struct.* **2020**, *218*, 110827. [CrossRef]
24. Kim, J.S.; Kwark, J.W.; Joh, C.B.; Yoo, S.W.; Lee, K.C. Headed stud shear connector for thin ultrahigh-performance concrete bridge deck. *J. Constr. Steel Res.* **2015**, *108*, 23–30. [CrossRef]
25. Wang, J.Q.; Qi, J.N.; Tong, T.; Xu, Q.Z.; Xiu, H.L. Static behavior of large stud shear connectors in steel-UHPC composite structures. *Eng. Struct.* **2019**, *178*, 534–542. [CrossRef]
26. Zou, Y.; Guo, J.C.; Zhou, Z.X.; Wang, X.D.; Yu, Y.J.; Zheng, K.D. Evaluation of shear behavior of PCSC shear connection for the construction of composite bridges with prefabricated decks. *Eng. Struct.* **2022**, *257*, 113870. [CrossRef]
27. Eurocode 4. *Design of Composite Steel and Concrete Structures*; European Committee for Standardization: Brussels, Belgium, 2004.
28. *GB/T50081-2016*; Standard for Test Methods for Mechanical Properties on Ordinary Concrete. China Construction Industry Press: Beijing, China, 2016.
29. *GB/T228-2010*; Standard for Metallic Materials-Tensile Testing-Part 1: Method of Test at Room Temperature. National Technical Management Committee of China: Beijing, China, 2010.
30. Zou, Y.; Yu, K.; Heng, J.L.; Zhang, Z.Y.; Peng, H.B.; Wu, C.l.; Wang, X.F. Feasibility study of new GFRP grid web—Concrete composite beam. *Compos. Struct.* **2023**, *305*, 116527. [CrossRef]
31. Japanese Society of Steel Construction. *Standard on Push-Out Test for Headed Stud (Draft)*; Japanese Society of Steel Construction: Tokyo, Japan, 1996. (In Japanese)
32. Wang, Y.C. Deflection of steel-concrete composite beams with partialshear interaction. *J. Struct. Eng.* **1998**, *124*, 1159–1165. [CrossRef]
33. Shim, C.S.; Lee, P.G.; Yoon, T.Y. Static behavior of large stud shear connectors. *Eng. Struct.* **2004**, *26*, 1853–1860. [CrossRef]
34. Lin, Z.F.; Liu, Y.Q.; He, J. Research on calculation method of shear stiffness for headed stud connectors. *Eng. Mech.* **2014**, *31*, 85–90.
35. Guo, J.C.; Zhou, Z.X.; Zou, Y.; Zhang, Z.Y.; Jiang, J.L.; Wang, X.D. Static behavior of novel shear connectors with post-poured UHPC for prefabricated composite bridge. *Structures* **2022**, *43*, 1114–1133. [CrossRef]
36. Zhang, Z.; Shao, X.; Li, W.; Zhu, P.; Chen, H. Axial tensile behavior test of ultra high performance concrete. *China J. Highw. Transp.* **2015**, *28*, 50–58.
37. Yang, J.; Fang, Z. Research on stress-strain relation of ultra high performance concrete. *Concrete* **2008**, *7*, 11–15.
38. Hibbitt, H.; Karlsson, B.; Sorensen, P. *Abaqus Analysis User's Manual Version 6.10*; Dassault Systèmes Simulia Corp.: Providence, RI, USA, 2011.